Table 4. Properties of the sources whose RV time series are compared with literature multi-epoch RV studies.

Name	*Gaia* DR3 source ID	Var. type[(a)]	Sp. type[(a)]	P_G(FPR) (days)	P_{V_R}(FPR) (days)	$P_{\mathrm{Lit.}}$ (days)	Reference
AR Cep	2300884800185315712	SRb	M4III	575.2	550.4		Alvarez et al. (2001)
RS CrB	1372316959598411520	SRa	M7	330.9	305.9	328.3 ± 2.6	Hinkle et al. (2002)
R Nor	5985676640941632384	Mira	M3e-M6II	505.5	496.7	507	Lebzelter et al. (2005a)

Notes. [(a)]The variability and spectral types are taken from the corresponding reference paper.

than the zero-point RV for the purpose of comparison as the values published in each of the three surveys we compare with are also derived as averages (unless coming from single-epoch observations).

We find comparable results for all three surveys, with a slightly higher degree of compatibility with APOGEE. The differences in RV are usually comparable with or smaller than the amplitude of RV variability. As expected, larger deviations occur for sources having large RV amplitudes, and therefore typically for ellipsoidal variables, as well as for sources with few observations in the examined external surveys. Indeed, the GALAH RVs for the matched sources are all based on single-epoch measurements. Of the sources matched with APOGEE, 29 are RVs based on single-epoch data, 52 have between 2 and 4 epoch spectra, and the remaining 8 sources have at most 8 spectral observations. Similarly, the vast majority of the sources matched with RAVE (1141) has a single epoch, while 70 have been observed during two epochs, and only 15 have more than two epochs (at most 7).

While the poor time coverage in the external surveys we compare with is the most likely cause of discrepancy with our RV values, another possible cause could be related with spectral mismatch, whether in the *Gaia* pipeline (as mentioned in Sect. 4.1.2) or in the literature survey. This seems to be the case, for example, for a few sources for which the RAVE catalog indicates effective temperatures in excess of 8000 K and that we identify as LPVs showing the largest RV differences compared to the FPR. We found no evident correlation between the RV differences and the differences between the spectral parameters adopted by the *Gaia* and external survey pipelines. A mismatch between the values of T_{eff} or $\log(g)$ does not necessarily lead to large RV differences, at least as long as these values are not unreasonably far from the range of stellar parameters typical of LPVs.

4.3.2. Comparison with literature multi-epoch RV data

There exist a limited number of literature studies providing multi-epoch RV data of LPVs and ellipsoidal variables, hence we found only three FPR sources that we could compare with published RV time series. They are summarized in Table 4, where the literature period is compared with the values P_G and P_{V_R} given in the FPR.

The first source for which we found a match is the SRb star AR Cep observed by Alvarez et al. (2001). They obtained spectral observations at optical wavelengths and derived RVs by cross-correlation with template spectra of types K0-III or M4-V. For the matched source they provide two RV epochs separated by about 2 months (roughly 10% of the period found in the *Gaia* time series). They found RVs between $-16.0\,\mathrm{km\,s^{-1}}$ and $-16.5\,\mathrm{km\,s^{-1}}$ (with little differences between the two spectral templates) that are in good agreement with our results, but they do not provide a period to compare with. Their RVs are shown on top of the *Gaia* RV curve folded with the best-fit RV model in the top section of Fig. 25 (an arbitrary phase offset is applied for the purpose of visual comparison). This source is not part of the TQS, and according to the criteria defined in Sect. 3 we identify it as a pulsating LPV.

Another source for which we found a match is the SRa star RS CrB, whose RV curve has been examined by Hinkle et al. (2002) based on near-IR spectral observations. They obtained measurements for 23 epochs spanning 5 yr, and derived a period of 328.3 ± 1.6 days that agrees with the value $P_G = 330.9$ days we derived from the G-band time series, but is less consistent with our RV period, $P_{V_R} = 305.9$ days. The time series of this source are compared in the middle section of Fig. 25, and in Fig. 26 we limit the comparison to the RV time series, folding them with both the FPR and literature RV periods. We note that both these periods are consistent with the longest of the three periods of RS CrB reported in literature, interpreted as resulting from binarity rather than pulsation. Indeed, the value given by Hinkle et al. (2002) is based on an orbital solution. Interestingly, we classify this source as a LPV but it lies very close to the boundary line defined by Eq. (10), so that its period is identified by pulsation. As clearly seen in Fig. 25, the photometric and RV time series of this source are consistent with each other, as a result this source is part of the TQS.

Finally, we found that the O-rich Mira R Nor is present both in the FPR and in the list of sources investigated by Lebzelter et al. (2005a). They derived RV measurements from nine near-IR spectra covering about an entire pulsation period of the star, for which they report a value of 507 days. This is in good agreement with both the periods we derived from the G-band and RV time series ($P_G = 505.5$ days, $P_{V_R} = 496.7$ days). The time series of this star are compared in the bottom section of Fig. 25. We identify this source as a pulsating LPV, but it is not part of the TQS.

It is worth noting that the RVs we are comparing for these three sources have been derived from different spectral ranges. Indeed, the observations by Alvarez et al. (2001) are taken at short wavelengths, between 390.6 nm and 681.1 nm, whereas the *Gaia* RVS covers the range between 846 nm and 870 nm. The spectral observations by Hinkle et al. (2002) and by Lebzelter et al. (2005a) cover an even more different range, being centered around 1.6 μm. This means that, if the observed variability results from pulsation, the RV measurements concern layers at different depths in the stellar atmosphere, and therefore the RV curves derived from different spectral ranges differ in terms of amplitude or show an offset between each other, which seems to be the case for R Nor (top-right panel in the bottom section of Fig. 25). While it should be kept in mind that the offset might be at least partially caused by a template mismatch in the processing of *Gaia* RVs (see Sect. 4.1.2), this figure clearly illustrates how such effects do not impact the quality of the RV variability parameters provided as part of this FPR. In the case of AR Cep

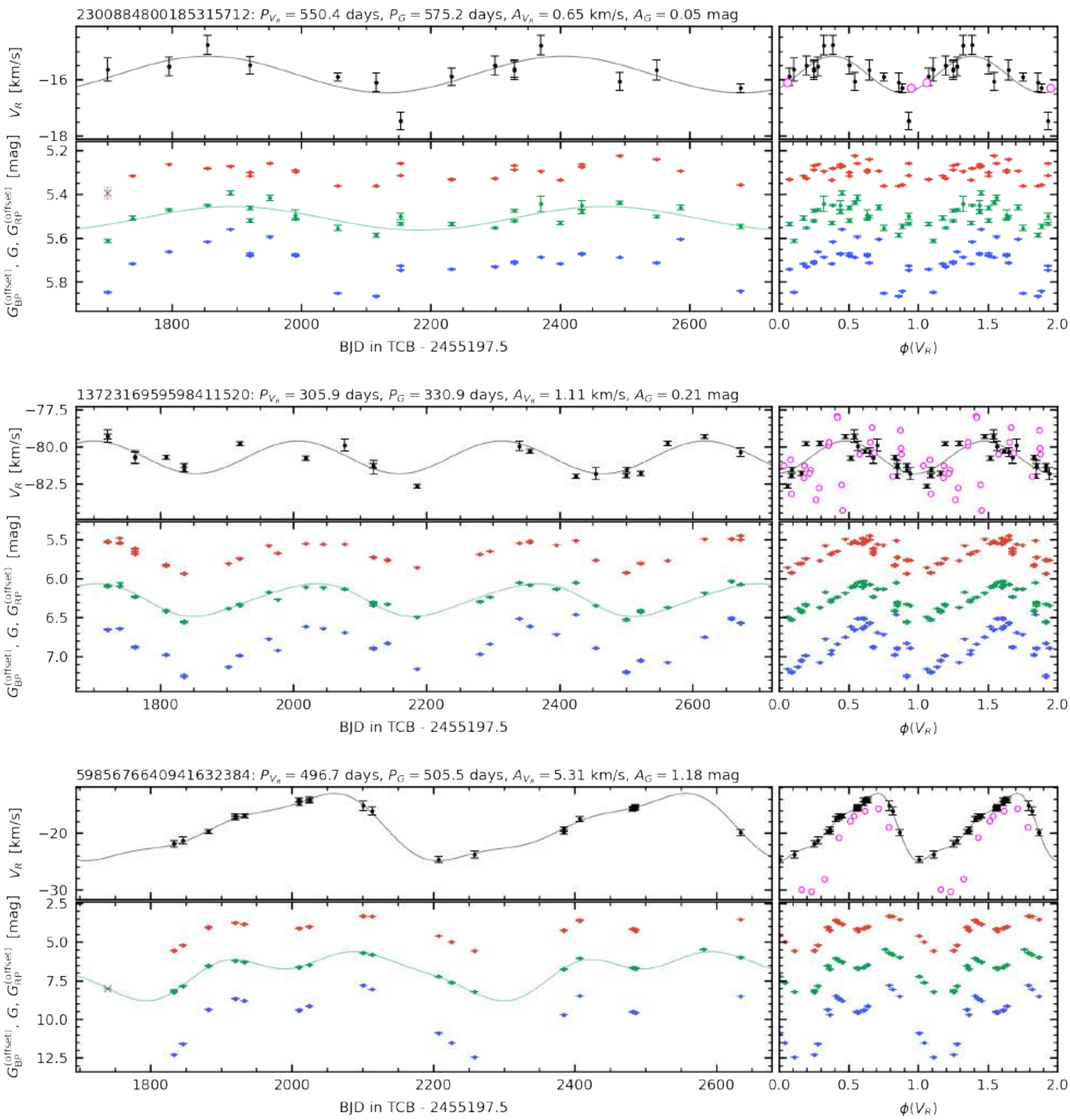

Fig. 25. Similar to Fig. 9, but showing the *Gaia* time series for the sources compared with literature as discussed in Sect. 4.3.2 (see also Table 4). The sources displayed from top to bottom are the SRb star AR Cep (compared with Alvarez et al. 2001), the binary SRa star RS CrB (compared with Hinkle et al. 2002), and the O-rich Mira R Nor (compared with Lebzelter et al. 2005a). Literature RV time series are displayed as magenta circles (with arbitrary phase offset) in the panels showing the folded RV curve. In each case, the *Gaia* RV period (indicated in the header of each panel) is used for folding.

(top section of Fig. 25) the small number of literature epochs to compare with makes it difficult to draw conclusions in this respect. In contrast, we note that the RV curves of RS CrB (middle section of Fig. 25) are well compatible in terms of average RV as well as amplitude (Fig. 26). This tends to confirm the orbital nature of the variability we detect for this source.

5. Catalog overview

In this section we provide an overview of the FPR catalog, with the purpose of showcasing its content of physical information. We first present the sky distribution of the catalog in Sect. 5.1, then investigate in Sect. 5.2 the distributions in the color – absolute magnitude diagram of subsets of sources with good relative parallax precisions, and finally analyze in Sect. 5.3 the period-luminosity relations of various subsets of the top-quality sample.

5.1. Sky distribution

Figure 27 illustrates the sky distribution of the sources in this FPR, each being color-coded by the median RV $\langle V_R \rangle$ resulting from the *Gaia* variability processing pipeline. As discussed in

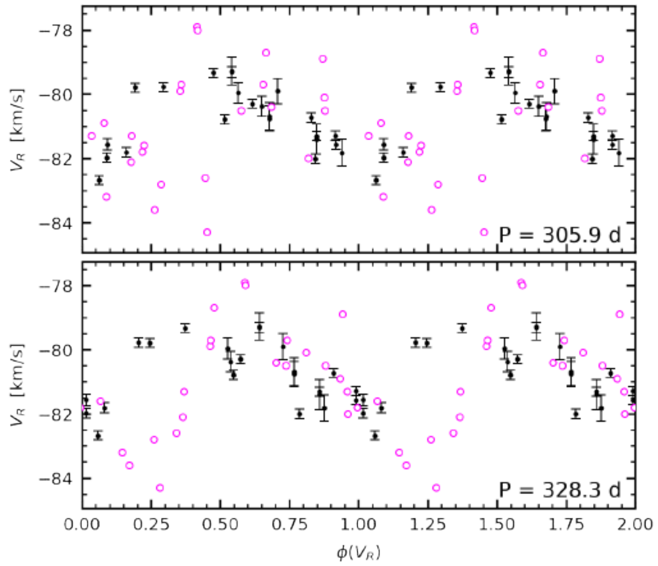

Fig. 26. Phased RV curve of RS CrB folded with the FPR RV period (top panel) and with the period derived by Hinkle et al. (2002; bottom panel). Symbols have the same meaning as in Fig. 25.

Sect. 4.1.1, for the vast majority of the FPR sources the value of $\langle V_R \rangle$ is compatible with the value of median RV derived from the *Gaia* spectroscopic data processing pipeline and published as part of *Gaia* DR3, even though the processing details are slightly different. Indeed, the physical picture emerging from Fig. 27 is entirely consistent with the expectations in terms of the Galactic rotation curve.

This also provides support to the expectation that the occurrence of spectral template mismatches has a minor impact on the accuracy of the median RV as an indicator of the center-of-mass velocity of the observed stars, even for the long-period, large-amplitude variables. We note that the RV difference between opposite parts of the Galaxy with respect to the Sun is $\gtrsim$200 km s^{-1}, which is much larger than any difference we encountered between $\langle V_R \rangle$ and the zero-point RV.

The sky distribution of the FPR shows some clear structures. Some of them are physical, such as the overdensity around the Galactic plane (but not on the plane itself, affected by strong interstellar extinction). The FPR contains a few sources located in the Small Magellanic Cloud (SMC) and Large Magellanic Cloud (LMC), with $V_R \sim 150$ km s^{-1} and $250 \lesssim V_R/\text{km s}^{-1} \lesssim 300$, respectively. Most (possibly all) of them are red supergiant stars, following the period-luminosity relation of fundamental-mode pulsators (see Sect. 5.3). However, some structures are artificial and result from the *Gaia* scanning law and the selection filters applied to construct the catalog. The most evident such structures are the lack of sources in the Galactic center, as well as the largely empty regions on the bottom-left and top-right parts of the map. These areas are aligned on the ecliptic, and are characterized by a relatively small number of *Gaia* transits. As a result, they are easily removed by our condition on the number of RV visibility periods (Sect. 2.1). Conversely, the "stripes" around the central hole correspond to fields of the sky often observed by *Gaia*.

5.2. Color–absolute magnitude diagram

We restrict the presentation in this section to the FPR sources having precise parallaxes, so that we can confidently derive their distance moduli μ and thus their absolute brightnesses. The distributions of the relative parallax errors for the FPR sample and various subsets thereof are displayed in Fig. 28 (excluding 92 sources with negative parallaxes). The results are largely independent on whether the sources are part of the TQS or not, whereas distinct distributions are observed for the different variability types present in the FPR. Indeed, ellipsoidal variables tend to have better parallax measurements than LPVs, and, within the latter category, LPVs showing an LSP have, on the average, slightly better parallax measurements than pulsating LPVs.

We set the upper limit on the relative parallax error at 15% (and require the parallax to be positive), thereby obtaining a sample of 5977 "good-parallax" sources (3740 in the TQS), that includes 794 ELL, 2136 pulsating LPVs, and 3047 LPVs showing a LSP. We examine this sample in the *Gaia* color – absolute magnitude diagram (CAMD, Fig. 29) constructed with the median magnitudes derived from the *Gaia* variability pipeline.

As expected, the majority of the LPVs are found on the asymptotic giant branch (AGB) of the CAMD, regardless of whether they show a LSP or a pulsation period. In contrast, ELL candidates are on the average fainter and bluer, and extend to the region of the red giant branch (RGB) in the CAMD. Most of the few stars with absolute G brighter than about 3 mag are identified as red supergiants (RSGs) in the SIMBAD astronomical database (Wenger et al. 2000), while some other ones could include massive AGB stars as well. Their periods tend to be identified as LSPs rather than pulsation by our classification method due to their relatively low variability amplitudes (see Sect. 3.2). Their true nature can clearly be revealed once their intrinsic brightness is known.

5.3. Period–luminosity diagrams

The sample can be further investigated in the period – luminosity diagram (PLD). To reveal the period – luminosity (PL) relations we adopt the *Gaia* Wesenheit index $W_{\mathrm{BP,RP}}$, which is an approximately reddening-free luminosity indicator (see Lebzelter et al. 2018, 2019, for the definition and details). We limit this analysis to the TQS in order to ensure higher period reliability, and note that we can construct two distinct PLDs depending on whether we adopt the period derived from photometric (taking here the G band) or RV time series. The two diagrams, both shown in Fig. 30, are entirely consistent with each other, except for the lower period limit, which is at 35 days for P_{V_R}, whereas it reaches $\sim$17.5 days for P_G due to the presence of sources with $P_{V_R} \simeq 2P_G$ in the sample.

The main features of the PLDs are the following. Regardless of the adopted period (P_G or P_{V_R}), pulsating LPVs are found primarily on the period-luminosity sequences C′ and C associated with pulsation in the first-overtone mode and fundamental mode, respectively (top panels in Fig. 30). Some of them, that we further examine below, have a period in the area of sequence D, which is associated with LSP variability (see e.g., Pawlak 2021, and references therein). A few of them have $P_G \lesssim 40$ days, possibly on the bright part of sequence B. These might be identified with the type of variables that, in the context of the Optical Gravitational Lensing Experiment (OGLE, Udalski et al. 1992), are known as OGLE Small-Amplitude Red Giants (OSARGs, Wray et al. 2004). The LPVs whose variability we identify as LSP, on the other hand, are mostly found on sequence D (middle panels in Fig. 30), except for the RSGs that are located on the bright end of sequence C. The RV periods of ellipsoidal red giants align on

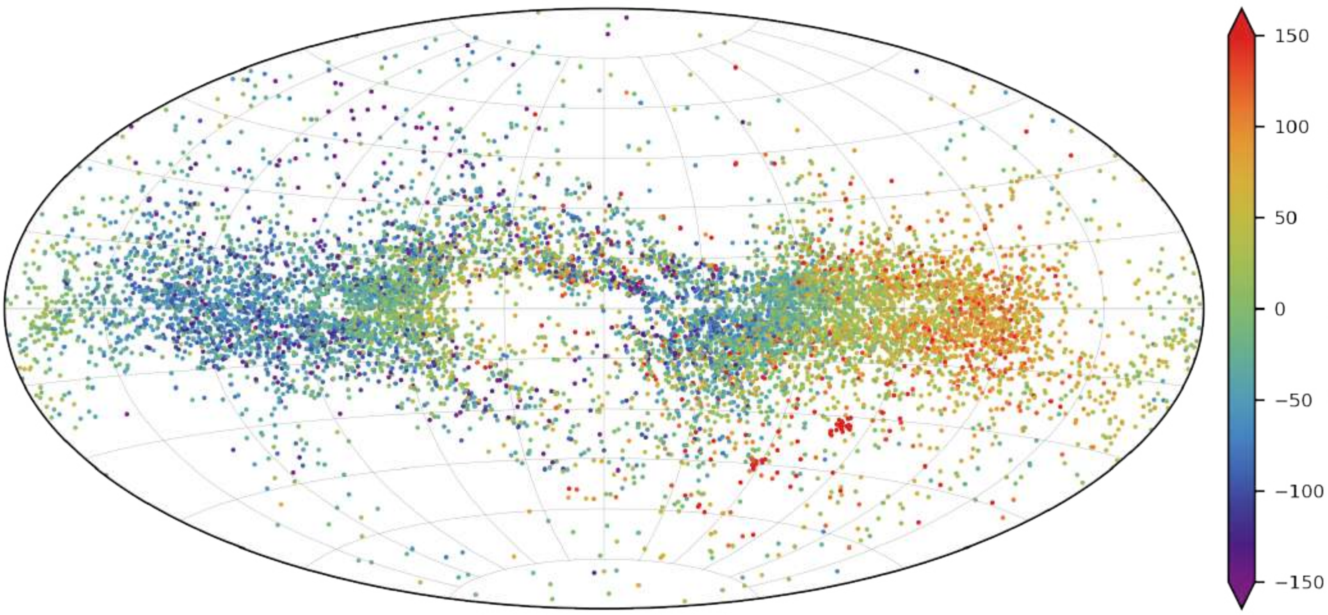

Fig. 27. Sky distribution in galactic coordinates of the sources in the FPR sample, color-coded by their median RV (the RV range is limited to 150 km s^{-1} in absolute value for visibility). The velocity pattern resulting from the rotation of the Milky Way Galaxy is clearly visible, as well as several bright sources in the Magellanic Clouds having $V_R \gtrsim 150\,\mathrm{km\,s^{-1}}$.

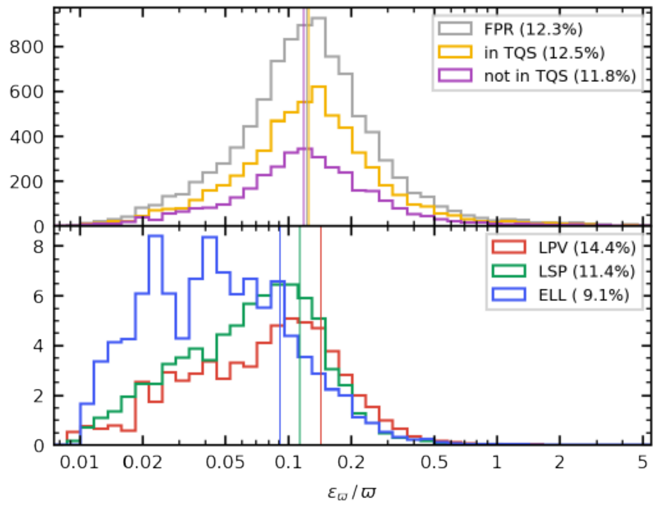

Fig. 28. Distribution of relative parallax errors in the FPR, excluding 92 sources with negative parallaxes. In the top panel, the histograms represent the full FPR (gray curve), the TQS (orange curve), and the sources that are not part of the TQS (purple). In the bottom panel, they indicate the sources identified as pulsating LPVs (red), LPVs showing a LSP (green), or ELL (blue). Note that the histograms in the bottom panel are normalized to their area. For each subset, the vertical line indicates the median relative error, which is reported as a percentage in the legends.

the PL sequence E (bottom panels in the figure), that forms a continuity with sequence D (see Fig. 1 of Soszyński et al. 2007).

In order to understand the presence of pulsation periods of LPVs on the PLD sequence D we have to distinguish between stars having O-rich and C-rich surface chemistry. Indeed, the PL relations corresponding to these two chemical types are different when examined through an optical-band Wesenheit index such as $W_{\mathrm{BP,RP}}$. A similar effect can be seen, for instance, in Fig. 1 of Soszyński et al. (2007; see also Lebzelter et al. 2018, 2019). To identify potential C-stars among the FPR sources we take advantage of the `is_cstar` flag provided with the *Gaia* DR3 catalog of LPV candidates (Lebzelter et al. 2023). About 7% of the FPR sources are classified as C-stars by this method, whereas 86% are identified as O-rich (another 7% are unclassified). After limiting the sample to pulsating LPV stars from the TQS and having good parallaxes, we find that 836 of them are O-rich, and 143 are C-rich. They are displayed in the PLD in Fig. 31, constructed using the photometric period P_G. In order to provide a visual reference for the positions of the PL relations, in the same diagrams we also show the sources from the OGLE-III catalog of LPVs in the LMC published by Soszyński et al. (2009). These authors also provide a photometry-based spectral-type classification which we use to discriminate between the O-rich and C-rich OGLE-III LPVs in Fig. 31.

As can be seen from the top panel of Fig. 31, there are some O-rich stars that we identified as pulsating LPVs and whose periods lie on the short-period, faint end of sequence D. These are LSPs mistakenly identified as pulsation periods by applying Eq. (10) because they lie close to the dividing line (between about 200 and 400 days, see Fig. 11). Let us now consider the C-rich sources in the bottom panel of Fig. 31. For the purpose of clear visualization, we do not show the C-rich OGLE sources whose primary period is flagged as a LSP. Indeed, the C-rich LPVs pulsating in the fundamental mode often lie below the corresponding PL relation (sequence C), overlapping with sequence D. This is a consequence of self-extinction by circumstellar dust which causes these sources to appear fainter than less dusty stars having similar periods (see e.g., Lebzelter et al. 2019, and references therein). This seems to be the case for the C-stars in our selection. Therefore, the presence of pulsating stars on sequence D can be correct if it results from circumstellar extinction.

Finally, we consider the TQS sources with good parallaxes and with $P_{V_R} \simeq 2\,P_G$. These are displayed in the PLDs in Fig. 32, constructed with P_G (top panel) and P_{V_R} (bottom panel). It is clear that the majority of these sources obey the PL relation E of

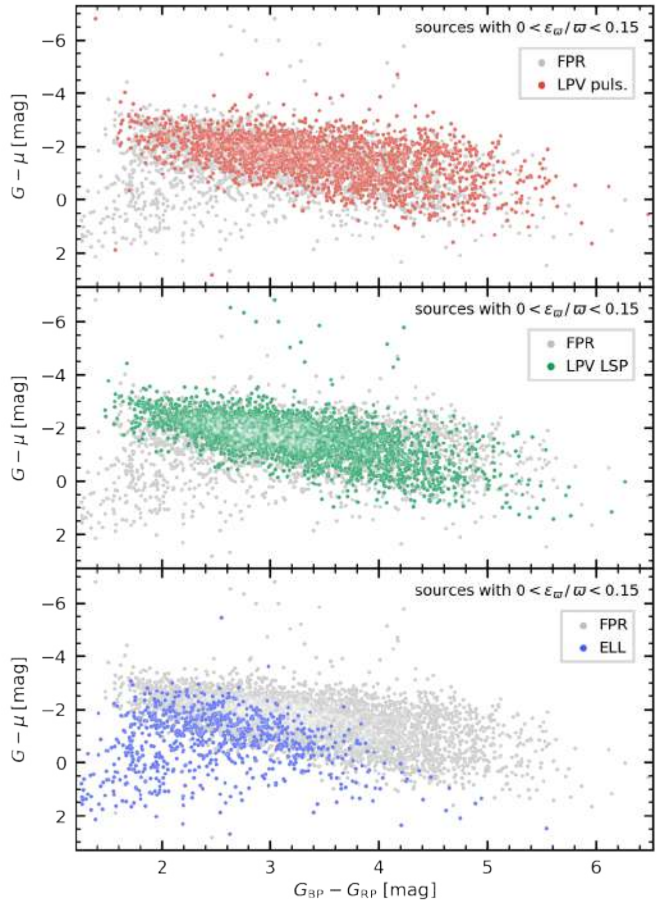

Fig. 29. *Gaia* color–absolute magnitude diagram of the FPR sources with positive parallaxes and parallax errors smaller than 15% (gray symbols), with μ being the distance modulus. The subsets of sources with different variability types are highlighted in the top (pulsating LPVs, red symbols), middle (LPVs with a LSP, green symbols) and bottom panels (ELL, blue symbols).

ellipsoidal red giants, leaving little doubt on the nature of their variability. Nonetheless, some of them populate other regions of the PLD, in particular the pulsation sequences C and C′ (and possibly B), as well as the LSP sequence D. This contradicts the naive expectation that the occurrence of P_{V_R} and P_G in a 2:1 ratio must indicate binary-induced variability. Let us then focus on the sources showing this feature and classified as LPVs (both pulsating and showing a LSP), which are highlighted in color in Fig. 32.

To begin with, we consider the *G*-band periods shorter than about 35 days, that are possibly compatible with the bright end of sequence B and that correspond to RV periods in the middle of sequence C′. If these periods are correct, it could mean that the variability pipeline identified the signature of first-overtone mode pulsation in the RV time series, and of second-overtone mode pulsation in the *G*-band time series. This would be consistent with the fact that, upon visual inspection, their photometric time series appear poorly regular, which can be taken as an indication of multi-periodicity. However, the first-overtone and second-overtone modes do not occur in a 2:1 ratio in LPVs (e.g., Wood 2015, and references therein). Furthermore, both sequences B and C′ are actually thought to result from pulsation in the first overtone mode (Trabucchi et al. 2017; Yu et al. 2020). Another explanation could be that these short *G*-band periods are associated with spurious frequencies resulting from scan-angle dependent signals (Holl et al. 2023). However, the origin of these spurious frequencies as described in that paper should affect only the *G* band and not the G_{BP} and G_{RP} measurements. Yet another explanation could be that the periods derived from the RV time series are not correct. We note that this kind of stars often display irregular variations that may result in the detection of spurious periods.

Entirely similar arguments can be put forward for the *G*-band periods along sequence C′ in the top panel of Fig. 32 (between about 40 and 200 days), which correspond to RV periods on sequence C, in the range 80–500 days. However, in this case it is more likely that they actually correspond, respectively, to the first-overtone mode and fundamental mode periods, which can occur in a 2:1 ratio Soszyński et al. (see e.g., Fig. 6 of 2007). The photometric and RV periods would then both be correct and consistent with a pulsational origin.

Finally, we consider the LPVs that appear on sequence D in either panel of Fig. 32. The vast majority of them are probably LSPs, even though some are identified as pulsating LPVs (red points in the figure). Indeed, as discussed above, they could be pulsating C-rich stars suffering from circumstellar extinction, but only a few of the sources shown in Fig. 32 are classified as probable C-stars. Another explanation for these stars showing $P_{V_R} \simeq 2\,P_G$ is that their LSPs are indeed caused by binarity, which would be consistent with the scenario outlined by Soszyński et al. (2021).

6. Summary and conclusions

The *Gaia* DR3 saw the publication of average RVs for over 33 million stars based on 34 months of observations with the *Gaia* RVS, whereas epoch radial velocities were published only for a very restricted list of variable sources. Anticipating the publication of the full RV data with the fourth *Gaia* data release, we present RV time series for a selected sample of long-period variables as part of this *Gaia* FPR.

We describe the construction of the catalog, starting with the set of *Gaia* LPV candidates with a median RV published in *Gaia* DR3, and applying several filtering steps to ensure the highest quality of the final sample, leading to 9614 sources. In addition to the RV time series, for each source we provide the model-derived frequency and amplitude of RV variability, as well as the RV statistics, determined by the *Gaia* variability processing pipeline. In addition, we publish a flag allowing for the identification of a subset of 6093 sources that show a high degree of compatibility between the periods derived from the RV and photometric time series. We consider them to be of superior quality as all four of their *Gaia* time series (three photometric bands and the RV channel) are likely to carry a strong signature from the same physical process, enabling detailed studies of their variability.

We show how the catalog includes three groups of sources exhibiting different types of variability, namely ellipsoidal red giants, pulsating LPVs, and LPVs displaying a long secondary period. Stars from the first group are characterized by comparatively large RV amplitudes (that cannot be attained by pulsating stars) and small photometric amplitudes. They also frequently show RV periods that are twice as long as the periods derived from the photometric time series. They represent between 10 to 15% of the catalog. The remainder of the FPR consists in roughly equal parts of LPVs showing pulsation and long secondary periods, which we tentatively distinguish by their different positions in the period-amplitude diagram.

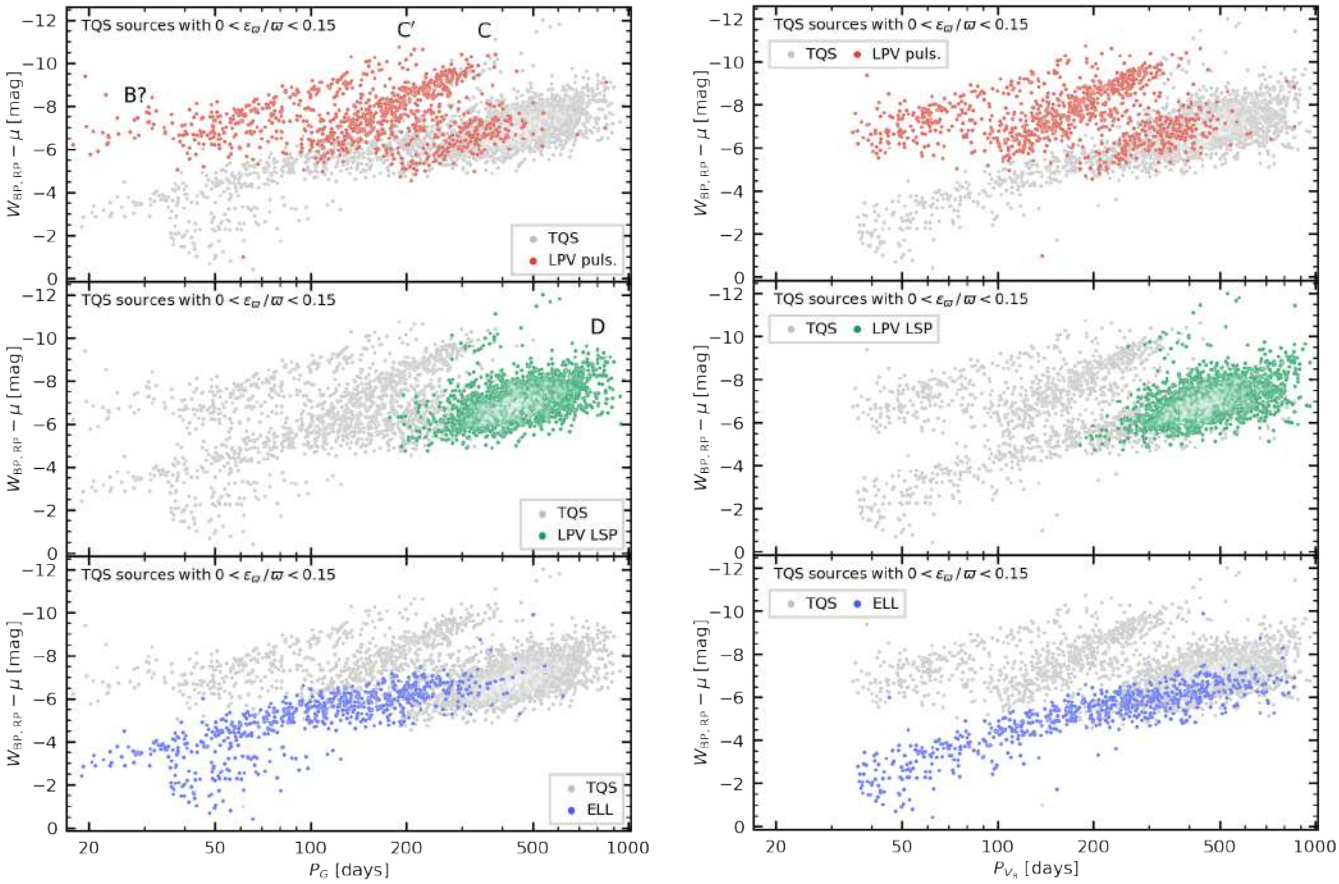

Fig. 30. Similar to Fig. 29, but showing the period – luminosity diagram. The panels in the left- and right-hand side columns employ the periods derived from the *G*-band and V_R time series, respectively, and the *Gaia* Wesenheit index $W_{BP,RP}$ is used as brightness indicator. The extent of the horizontal axis is intentionally kept the same in all panels for the purpose of comparison.

We further verify the quality of the FPR by comparison with *Gaia* DR3 products as well as other literature data. We show that, despite the use of a different pipeline, the median RV derived by our variability processing is entirely consistent with previous *Gaia* data.

When using the median RV of LPVs as a measure of the systemic velocity, one has to consider the following limitations. The first one is connected to the uneven time sampling of *Gaia* observations. Combined with the long periods and large amplitudes of the sources we examined, it can lead to a substantial degree of undersampling of specific phases of the variability cycle, skewing the RV distribution away from the true systemic velocity. In this case, the maximum uncertainty is given by half the peak-to-peak (true) RV variability amplitude. The occurrence of multi-periodicity might affect the median in a similar way.

The second limitation is connected with the possibly asymmetric shape of the RV curves of pulsating LPVs, in which case the median does not necessarily trace the systemic velocity, regardless of the sampling. Once again, the maximum deviation cannot be larger than half the peak-to-peak RV amplitude. Finally, a limitation could arise from the possible occurrence of template mismatches, that is the adoption, for the purpose of deriving RVs, of a spectral template whose atmospheric parameters are not suited for the target star. LPVs with C-rich chemistry, whose spectra show very distinctive molecular absorption features, are especially exposed to this risk, as all the adopted templates are for O-rich composition. In this case, it is not easy to assess the maximum deviation. However, our analysis suggests that none of these three aspects significantly affect the RV variability parameters published here.

We then present an overview of the catalog. We first show that the distribution of the RVs on the sky is physically consistent with the Galactic rotation curve. We then analyze, in the color – absolute magnitude diagram and in the period – luminosity diagram, the distribution of a subsample with good parallaxes. The sources identified as LPVs showing a LSP and as ellipsoidal variables by our classification scheme are seen to follow the period-luminosity relations D and E, respectively, as expected. The periods of pulsating LPVs, on the other hand, are found mainly on sequences C′ and C, corresponding to the first-overtone mode and the fundamental mode, respectively. Some of these sources show a 2:1 ratio between the RV period and the photometric period, which is consistent with simultaneous pulsation in those two modes. These results indicate the rich content of physical information available in both the RV and photometric time series.

This FPR includes the largest dataset of RV time series of LPVs to date. Moreover, it covers sources over a largely unexplored (in terms of RV time-series analysis) range of distances, intermediate between the extragalactic investigations of variable stars in the Magellanic Clouds and the studies of nearby LPVs. The RV time series, together with the photometric time series published in *Gaia* DR3 and spanning the same time baseline, offer an unprecedented opportunity to investigate, from different perspectives, the behavior of three different types of red giant variables, including the LSPs whose nature is still a matter of

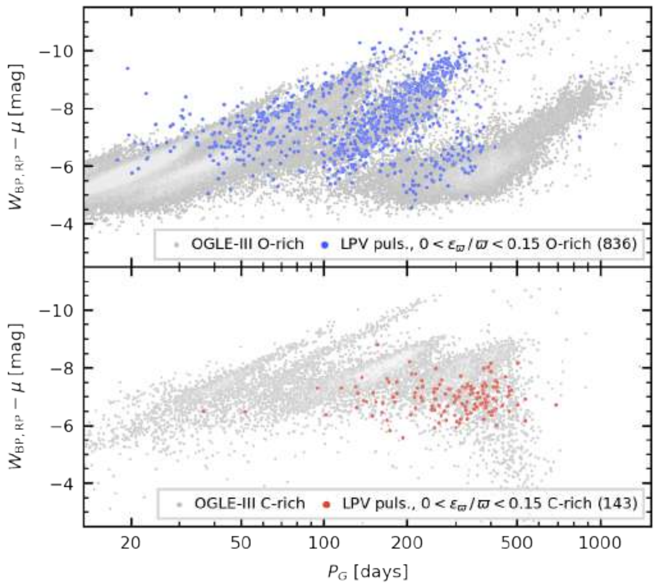

Fig. 31. Similar to the Fig. 30, but limited to pulsating LPVs and distinguishing between sources identified as C-stars (red symbols, bottom panel) or not (blue symbols, top panel) according to *Gaia* low-resolution spectra (Lebzelter et al. 2023). The numbers of these sources are indicated in the legends. Gray points in the background are O-rich (top panel) or C-rich (bottom panel) LPVs in the LMC from the OGLE-III catalog (sources whose OGLE primary period is flagged as LSP are excluded from the bottom panel). For the LMC, we adopt an average distance modulus $\mu_{\rm LMC}$ = 18.49 mag following de Grijs et al. (2017).

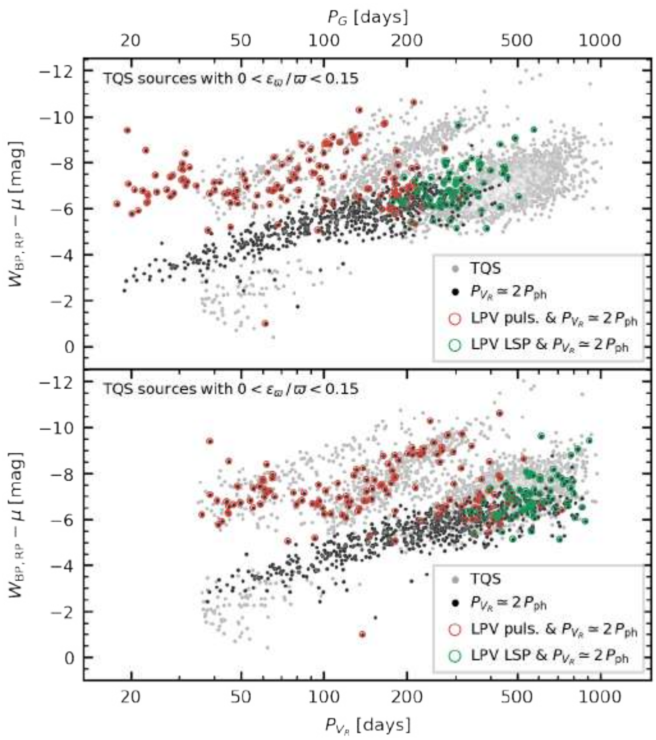

Fig. 32. Similar to the right-hand side panels in Fig. 30, but with the sources having $P_{V_R} \simeq 2P_{\rm ph}$ highlighted in black. The PLD constructed with P_G is shown in the top panel and the one constructed with P_{V_R} in the bottom panel for the TQS sources with parallax errors better than 15% (gray symbols), and highlighting the sources with $P_{V_R} \simeq 2P_{\rm ph}$. Red and green circles indicate LPVs showing pulsation and a LSP, respectively. Only five of them are identified as C-rich.

debate. Finally, the high-quality epoch RV data of this FPR will provide the astrophysical community with a means to prepare for the *Gaia* data release 4.

Acknowledgements. This work presents results from the European Space Agency (ESA) space mission *Gaia*. *Gaia* data are being processed by the *Gaia* Data Processing and Analysis Consortium (DPAC). Funding for the DPAC is provided by national institutions, in particular the institutions participating in the *Gaia* MultiLateral Agreement (MLA). The *Gaia* mission website is https://www.cosmos.esa.int/gaia. The *Gaia* archive website is https://archives.esac.esa.int/gaia. Full acknowledgements are given in Appendix E.

References

Ahn, C. P., Alexandroff, R., Allende Prieto, C., et al. 2012, ApJS, 203, 21
Alvarez, R., Jorissen, A., Plez, B., et al. 2001, A&A, 379, 305
Albareti, F. D., Allende Prieto, C., Almeida, A., et al. 2017, ApJS, 233, 25
Astropy Collaboration (Price-Whelan, A., et al.) 2018, AJ, 156, 123
Boch, T., & Fernique, P. 2014, in Astronomical Society of the Pacific Conference Series, 485, Astronomical Data Analysis Software and Systems XXIII, eds. N. Manset, & P. Forshay, 277
Bonnarel, F., Fernique, P., Bienaymé, O., et al. 2000, A&AS, 143, 33
Breddels, M. A., & Veljanoski, J. 2018, A&A, 618, A13
Buder, S., Sharma, S., Kos, J., et al. 2021, MNRAS, 506, 150
Chambers, K. C., Magnier, E. A., Metcalfe, N., et al. 2016, ArXiv e-prints
Clementini, G., Ripepi, V., Garofalo, A., et al. 2023, A&A, 674, A18
de Grijs, R., Courbin, F., Martínez-Vázquez, C. E., et al. 2017, Space Sci. Rev., 212, 1743
Eyer, L., Mowlavi, N., Evans, D. W., et al. 2017, arXiv e-prints [arXiv:1702.03295]
Eyer, L., Audard, M., Holl, B., et al. 2023, A&A, 674, A13
Fabricius, C., Høg, E., Makarov, V. V., et al. 2002, A&A, 384, 180
Flewelling, H. A., Magnier, E. A., Chambers, K. C., et al. 2020, ApJS, 251, 7
Gaia Collaboration (Vallenari, A., et al.) 2023, A&A, 674, A1
Gilmore, G., Randich, S., Worley, C. C., et al. 2022, A&A, in press
Górski, K. M., Hivon, E., Banday, A. J., et al. 2005, ApJ, 622, 759
Henden, A. A., Templeton, M., Terrell, D., et al. 2016, VizieR Online Data Catalogue: 2336
Hinkle, K. H., & Barnbaum, C. 1996, AJ, 111, 913
Hinkle, K. H., & Barnes, T. G. 1979, ApJ, 234, 548
Hinkle, K. H., Hall, D. N. B., & Ridgway, S. T. 1982, ApJ, 252, 697
Hinkle, K. H., Scharlach, W. W. G., & Hall, D. N. B. 1984, ApJS, 56, 1
Hinkle, K. H., Lebzelter, T., Joyce, R. R., & Fekel, F. C. 2002, AJ, 123, 1002
Hinkle, K. H., Fekel, F. C., Joyce, R. R., & Wood, P. 2013, ApJ, 770, 28
Høg, E., Fabricius, C., Makarov, V. V., et al. 2000, A&A, 355, L27
Höfner, S., & Olofsson, H. 2018, A&ARv, 26, 1
Holl, B., Fabricius, C., Portell, J., et al. 2023, A&A, 674, A25
Huber, D., Bryson, S. T., Haas, M. R., et al. 2016, ApJS, 224, 2
Hunter, J. D. 2007, Comput. Sci. Eng., 9, 90
Jönsson, H., Holtzman, J. A., Allende Prieto, C., et al. 2020, AJ, 160, 120
Joy, A. H. 1926, ApJ, 63, 281
Joy, A. H. 1954, ApJS, 1, 39
Katz, D., Sartoretti, P., Guerrier, A., et al. 2023, A&A, 674, A5
Lasker, B. M., Lattanzi, M. G., McLean, B. J., et al. 2008, AJ, 136, 735
Lebzelter, T. 1999, A&A, 351, 644
Lebzelter, T., & Hinkle, K. H. 2002, ASP Conf. Ser., 259, 556
Lebzelter, T., Hinkle, K. H., & Hron, J. 1999, A&A, 341, 224
Lebzelter, T., Hinkle, K. H., Wood, P. R., Joyce, R. R., & Fekel, F. C. 2005a, A&A, 431, 623
Lebzelter, T., Wood, P. R., Hinkle, K. H., Joyce, R. R., & Fekel, F. C. 2005b, A&A, 432, 207
Lebzelter, T., Mowlavi, N., Marigo, P., et al. 2018, A&A, 616, L13
Lebzelter, T., Trabucchi, M., Mowlavi, N., et al. 2019, A&A, 631, A24
Lebzelter, T., Mowlavi, N., Lecoeur-Taibi, I., et al. 2023, A&A, 674, A15
Luo, A. L., Zhao, Y.-H., Zhao, G., et al. 2015, Res. Astron. Astrophys., 15, 1095
Magnier, E. A., Chambers, K. C., Flewelling, H. A., et al. 2020a, ApJS, 251, 3
Magnier, E. A., Schlafly, E. F., Finkbeiner, D. P., et al. 2020b, ApJS, 251, 6
Magnier, E. A., Sweeney, W. E., Chambers, K. C., et al. 2020c, ApJS, 251, 5
Mowlavi, N. 2014, A&A, 568, A78
Mowlavi, N., Lecoeur-Taïbi, I., Holl, B., et al. 2017, A&A, 606, A92
Mowlavi, N., Lecoeur-Taïbi, I., Lebzelter, T., et al. 2018, A&A, 618, A58
Mowlavi, N., Holl, B., Lecoeur-Taïbi, I., et al. 2023, A&A, 674, A16
Nicholls, C. P., Wood, P. R., & Cioni, M. R. L. 2010, MNRAS, 405, 1770
Nie, J. D., & Wood, P. R. 2014, AJ, 148, 118
Nie, J. D., Wood, P. R., & Nicholls, C. P. 2017, ApJ, 835, 209
Nowotny, W., Höfner, S., & Aringer, B. 2010, A&A, 514, A35

Ochsenbein, F., Bauer, P., & Marcout, J. 2000, A&AS, 143, 23
Onken, C. A., Wolf, C., Bessell, M. S., et al. 2019, PASA, 36, e033
Pawlak, M. 2021, A&A, 649, A110
Pérez, F., & Granger, B. E. 2007, Comput. Sci. Eng., 9, 21
Randich, S., Gilmore, G., Magrini, L., et al. 2022, A&A, in press
R Core Team 2013, R: A Language and Environment for Statistical Computing (Vienna, Austria: R Foundation for Statistical Computing)
Reid, M. J., & Dickinson, D. F. 1976, ApJ, 209, 505
Reid, M. J., & Goldston, J. E. 2002, ApJ, 568, 931
Ripepi, V., Clementini, G., Molinaro, R., et al. 2023, A&A, 674, A17
Roeser, S., Demleitner, M., & Schilbach, E. 2010, AJ, 139, 2440
Saio, H., Wood, P. R., Takayama, M., & Ita, Y. 2015, MNRAS, 452, 3863
Sartoretti, P., Blomme, R., David, M., & Seabroke, G. 2022, Gaia DR3 documentation Chapter 6: Spectroscopy, *Gaia* DR3 documentation, European Space Agency; *Gaia* Data Processing and Analysis Consortium. Online at `gea.esac.esa.int/archive/documentation/GDR3/index.html`, id. 6
Sartoretti, P., Marchal, O., Babusiaux, C., et al. 2023, A&A, 674, A6
Seaquist, E. R., & Taylor, A. R. 1990, ApJ, 349, 313
Skrutskie, M. F., Cutri, R. M., Stiening, R., et al. 2006, AJ, 131, 1163
Steinmetz, M., Guiglion, G., McMillan, P. J., et al. 2020a, AJ, 160, 83
Steinmetz, M., Matijevič, G., Enke, H., et al. 2020b, AJ, 160, 82
Soszyński, I., & Udalski, A. 2014, ApJ, 788, 13
Soszyński, I., Udalski, A., Kubiak, M., et al. 2004, Acta Astron., 54, 347
Soszyński, I., Dziembowski, W. A., Udalski, A., et al. 2007, Acta Astron., 57, 201
Soszyński, I., Udalski, A., Szymański, M. K., et al. 2009, Acta Astron., 59, 239
Soszyński, I., Olechowska, A., Ratajczak, M., et al. 2021, ApJ, 911, L22
Steinmetz, M., Matijevič, G., Enke, H., et al. 2020, AJ, 160, 82
Taylor, M. B. 2005, in Astronomical Society of the Pacific Conference Series, 347, Astronomical Data Analysis Software and Systems XIV, eds. P. Shopbell, M. Britton, & R. Ebert, 29
Taylor, M. B. 2006, in Astronomical Society of the Pacific Conference Series, 351, Astronomical Data Analysis Software and Systems XV, eds. C. Gabriel, C. Arviset, D. Ponz, & S. Enrique, 666
Trabucchi, M., Wood, P. R., Montalbán, J., et al. 2017, ApJ, 847, 139
Udalski, A., Szymanski, M., Kaluzny, J., Kubiak, M., & Mateo, M. 1992, Acta Astron., 42, 253
van Leeuwen, F. 2007, A&A, 474, 653
Wallerstein, G. 1985, PASP, 97, 994
Waters, C. Z., Magnier, E. A., Price, P. A., et al. 2020, ApJS, 251, 4
Wenger, M., Ochsenbein, F., Egret, D., et al. 2000, A&AS, 143, 9
Wood, P. R. 2015, MNRAS, 448, 3829
Wood, P. R. 2000, PASA, 17, 18
Wood, P. R., & Sebo, K. M. 1996, MNRAS, 282, 958
Wray, J. J., Eyer, L., & Paczyński, B. 2004, MNRAS, 349, 1059
Yu, J., Bedding, T. R., Stello, D., et al. 2020, MNRAS, 493, 1388
Zacharias, N., Finch, C. T., Girard, T. M., et al. 2013, AJ, 145, 44
Zacharias, N., Finch, C., Subasavage, J., et al. 2015, AJ, 150, 101

[1] Department of Physics and Astronomy G. Galilei, University of Padova, Vicolo dell'Osservatorio 3, 35122 Padova, Italy
[2] Department of Astronomy, University of Geneva, Chemin Pegasi 51, 1290 Versoix, Switzerland
[3] University of Vienna, Department of Astrophysics, Türkenschanzstraße 17, 1180 Vienna, Austria
[4] Department of Astronomy, University of Geneva, Chemin d'Ecogia 16, 1290 Versoix, Switzerland
[5] European Space Agency (ESA), European Space Astronomy Centre (ESAC), Camino bajo del Castillo s/n, Urbanización Villafranca del Castillo, Villanueva de la Cañada, 28692 Madrid, Spain
[6] RHEA for European Space Agency (ESA), Camino bajo del Castillo s/n, Urbanización Villafranca del Castillo, Villanueva de la Cañada, 28692 Madrid, Spain
[7] Sednai Sàrl, 1204 Geneva, Switzerland
[8] GEPI, Observatoire de Paris, Université PSL, CNRS, 5 place Jules Janssen, 92190 Meudon, France
[9] Royal Observatory of Belgium, Ringlaan 3, 1180 Brussels, Belgium
[10] Université de Strasbourg, CNRS, Observatoire astronomique de Strasbourg, UMR 7550, 11 rue de l'Université, 67000 Strasbourg, France
[11] Institut d'Astrophysique et de Géophysique, Université de Liège, 19c, Allée du 6 Août, 4000 Liège, Belgium
[12] CRAAG – Centre de Recherche en Astronomie, Astrophysique et Géophysique, Route de l'Observatoire, BP 63, Bouzareah 16340, Algiers, Algeria
[13] Leiden Observatory, Leiden University, Niels Bohrweg 2, 2333 CA Leiden, The Netherlands
[14] CNES Centre Spatial de Toulouse, 18 avenue Édouard Belin, 31401 Toulouse Cedex 9, France
[15] Mullard Space Science Laboratory, University College London, Holmbury St Mary, Dorking, Surrey RH5 6NT, UK
[16] INAF – Osservatorio astronomico di Padova, Vicolo Osservatorio 5, 35122 Padova, Italy
[17] European Space Agency (ESA), European Space Research and Technology Centre (ESTEC), Keplerlaan 1, 2201AZ, Noordwijk, The Netherlands
[18] Univ. Grenoble Alpes, CNRS, IPAG, 38000 Grenoble, France
[19] Astronomisches Rechen-Institut, Zentrum für Astronomie der Universität Heidelberg, Mönchhofstr. 12–14, 69120 Heidelberg, Germany
[20] Université Côte d'Azur, Observatoire de la Côte d'Azur, CNRS, Laboratoire Lagrange, Bd de l'Observatoire, CS 34229, 06304 Nice Cedex 4, France
[21] Laboratoire d'astrophysique de Bordeaux, Univ. Bordeaux, CNRS, B18N, allée Geoffroy Saint-Hilaire, 33615 Pessac, France
[22] Institute of Astronomy, University of Cambridge, Madingley Road, Cambridge CB3 0HA, UK
[23] Aurora Technology for European Space Agency (ESA), Camino bajo del Castillo s/n, Urbanización Villafranca del Castillo, Villanueva de la Cañada, 28692 Madrid, Spain
[24] Institut de Ciències del Cosmos (ICCUB), Universitat de Barcelona (UB), Martí i Franquès 1, 08028 Barcelona, Spain
[25] Departament de Física Quàntica i Astrofísica (FQA), Universitat de Barcelona (UB), c. Martí i Franquès 1, 08028 Barcelona, Spain
[26] Institut d'Estudis Espacials de Catalunya (IEEC), c. Gran Capità 2–4, 08034 Barcelona, Spain
[27] Lohrmann Observatory, Technische Universität Dresden, Mommsenstraße 13, 01062 Dresden, Germany
[28] Lund Observatory, Division of Astrophysics, Department of Physics, Lund University, Box 43, 22100 Lund, Sweden
[29] INAF – Osservatorio Astrofisico di Arcetri, Largo Enrico Fermi 5, 50125 Firenze, Italy
[30] Nicolaus Copernicus Astronomical Center, Polish Academy of Sciences, ul. Bartycka 18, 00-716 Warsaw, Poland
[31] Max Planck Institute for Astronomy, Königstuhl 17, 69117 Heidelberg, Germany
[32] INAF – Osservatorio Astrofisico di Torino, via Osservatorio 20, 10025 Pino Torinese (TO), Italy
[33] University of Turin, Department of Physics, Via Pietro Giuria 1, 10125 Torino, Italy
[34] DAPCOM Data Services, c. dels Vilabella 5–7, 80500 Vic, Barcelona, Spain
[35] ALTEC S.p.a, Corso Marche 79,10146 Torino, Italy
[36] Gaia DPAC Project Office, ESAC, Camino bajo del Castillo s/n, Urbanización Villafranca del Castillo, Villanueva de la Cañada, 28692 Madrid, Spain
[37] Telespazio UK S.L. for European Space Agency (ESA), Camino bajo del Castillo s/n, Urbanización Villafranca del Castillo, Villanueva de la Cañada, 28692 Madrid, Spain
[38] SYRTE, Observatoire de Paris, Université PSL, CNRS, Sorbonne Université, LNE, 61 avenue de l'Observatoire, 75014 Paris, France
[39] IMCCE, Observatoire de Paris, Université PSL, CNRS, Sorbonne Université, Univ. Lille, 77 av. Denfert-Rochereau, 75014 Paris, France
[40] Serco Gestión de Negocios for European Space Agency (ESA), Camino bajo del Castillo s/n, Urbanización Villafranca del Castillo, Villanueva de la Cañada, 28692 Madrid, Spain
[41] INAF – Osservatorio di Astrofisica e Scienza dello Spazio di Bologna, via Piero Gobetti 93/3, 40129 Bologna, Italy

[42] Institute for Astronomy, University of Edinburgh, Royal Observatory, Blackford Hill, Edinburgh EH9 3HJ, UK
[43] CIGUS CITIC – Department of Computer Science and Information Technologies, University of A Coruña, Campus de Elviña s/n, A Coruña, 15071, Spain
[44] ATG Europe for European Space Agency (ESA), Camino bajo del Castillo s/n, Urbanización Villafranca del Castillo, Villanueva de la Cañada, 28692 Madrid, Spain
[45] Kavli Institute for Cosmology Cambridge, Institute of Astronomy, Madingley Road, Cambridge CB3 0HA, UK
[46] Department of Astrophysics, Astronomy and Mechanics, National and Kapodistrian University of Athens, Panepistimiopolis, Zografos, 15783 Athens, Greece
[47] Donald Bren School of Information and Computer Sciences, University of California, Irvine, CA 92697, USA
[48] CENTRA, Faculdade de Ciências, Universidade de Lisboa, Edif. C8, Campo Grande, 1749-016 Lisboa, Portugal
[49] INAF – Osservatorio Astrofisico di Catania, via S. Sofia 78, 95123 Catania, Italy
[50] Dipartimento di Fisica e Astronomia "Ettore Majorana", Università di Catania, Via S. Sofia 64, 95123 Catania, Italy
[51] INAF – Osservatorio Astronomico di Roma, Via Frascati 33, 00078 Monte Porzio Catone (Roma), Italy
[52] Space Science Data Center – ASI, Via del Politecnico SNC, 00133 Roma, Italy
[53] Department of Physics, University of Helsinki, PO Box 64, 00014 Helsinki, Finland
[54] Finnish Geospatial Research Institute FGI, Vuorimiehentie 5, 02150 Espoo, Finland
[55] Institut UTINAM CNRS UMR6213, Université de Franche-Comté, OSU THETA Franche-Comté Bourgogne, Observatoire de Besançon, BP1615, 25010 Besançon Cedex, France
[56] HE Space Operations BV for European Space Agency (ESA), Keplerlaan 1, 2201AZ, Noordwijk, The Netherlands
[57] Dpto. de Inteligencia Artificial, UNED, c/ Juan del Rosal 16, 28040 Madrid, Spain
[58] Institut d'Astronomie et d'Astrophysique, Université Libre de Bruxelles CP 226, Boulevard du Triomphe, 1050 Brussels, Belgium
[59] Leibniz Institute for Astrophysics Potsdam (AIP), An der Sternwarte 16, 14482 Potsdam, Germany
[60] Konkoly Observatory, Research Centre for Astronomy and Earth Sciences, Eötvös Loránd Research Network (ELKH), MTA Centre of Excellence, Konkoly Thege Miklós út 15–17, 1121 Budapest, Hungary
[61] ELTE Eötvös Loránd University, Institute of Physics, 1117, Pázmány Péter sétány 1A, Budapest, Hungary
[62] Instituut voor Sterrenkunde, KU Leuven, Celestijnenlaan 200D, 3001 Leuven, Belgium
[63] Department of Astrophysics/IMAPP, Radboud University, PO Box 9010, 6500 GL Nijmegen, The Netherlands
[64] Institute of Physics, Ecole Polytechnique Fédérale de Lausanne (EPFL), Observatoire de Sauverny, 1290 Versoix, Switzerland
[65] Quasar Science Resources for European Space Agency (ESA), Camino bajo del Castillo s/n, Urbanización Villafranca del Castillo, Villanueva de la Cañada, 28692 Madrid, Spain
[66] LASIGE, Faculdade de Ciências, Universidade de Lisboa, Edif. C6, Campo Grande, 1749-016 Lisboa, Portugal
[67] School of Physics and Astronomy , University of Leicester, University Road, Leicester LE1 7RH, UK
[68] School of Physics and Astronomy, Tel Aviv University, Tel Aviv 6997801, Israel
[69] Cavendish Laboratory, JJ Thomson Avenue, Cambridge CB3 0HE, UK
[70] Telespazio for CNES Centre Spatial de Toulouse, 18 avenue Édouard Belin, 31401 Toulouse Cedex 9, France
[71] National Observatory of Athens, I. Metaxa and Vas. Pavlou, Palaia Penteli, 15236 Athens, Greece
[72] Depto. Estadística e Investigación Operativa. Universidad de Cádiz, Avda. República Saharaui s/n, 11510 Puerto Real, Cádiz, Spain
[73] EURIX S.r.l., Corso Vittorio Emanuele II 61, 10128 Torino, Italy
[74] Porter School of the Environment and Earth Sciences, Tel Aviv University, Tel Aviv 6997801, Israel
[75] ATOS for CNES Centre Spatial de Toulouse, 18 avenue Édouard Belin, 31401 Toulouse Cedex 9, France
[76] HE Space Operations BV for European Space Agency (ESA), Camino bajo del Castillo s/n, Urbanización Villafranca del Castillo, Villanueva de la Cañada, 28692 Madrid, Spain
[77] LFCA/DAS, Universidad de Chile, CNRS, Casilla 36-D, Santiago, Chile
[78] SISSA – Scuola Internazionale Superiore di Studi Avanzati, via Bonomea 265, 34136 Trieste, Italy
[79] University of Turin, Department of Computer Sciences, Corso Svizzera 185, 10149 Torino, Italy
[80] Thales Services for CNES Centre Spatial de Toulouse, 18 avenue Édouard Belin, 31401 Toulouse Cedex 9, France
[81] Dpto. de Matemática Aplicada y Ciencias de la Computación, Univ. de Cantabria, ETS Ingenieros de Caminos, Canales y Puertos, Avda. de los Castros s/n, 39005 Santander, Spain
[82] Institut de Física d'Altes Energies (IFAE), The Barcelona Institute of Science and Technology, Campus UAB, 08193 Bellaterra (Barcelona), Spain
[83] Port d'Informació Científica (PIC), Campus UAB, C. Albareda s/n, 08193 Bellaterra (Barcelona), Spain
[84] Instituto de Astrofísica, Universidad Andres Bello, Fernandez Concha 700, Las Condes, Santiago RM, Chile
[85] Centre for Astrophysics Research, University of Hertfordshire, College Lane, AL10 9AB, Hatfield, UK
[86] University of Turin, Mathematical Department "G. Peano", Via Carlo Alberto 10, 10123 Torino, Italy
[87] University of Antwerp, Onderzoeksgroep Toegepaste Wiskunde, Middelheimlaan 1, 2020 Antwerp, Belgium
[88] INAF – Osservatorio Astronomico d'Abruzzo, Via Mentore Maggini, 64100 Teramo, Italy
[89] Instituto de Astronomia, Geofìsica e Ciências Atmosféricas, Universidade de São Paulo, Rua do Matão 1226, Cidade Universitaria, 05508-900 São Paulo, SP, Brazil
[90] Mésocentre de calcul de Franche-Comté, Université de Franche-Comté, 16 route de Gray, 25030 Besançon Cedex, France
[91] Ruđer Bošković Institute, Bijenička cesta 54, 10000 Zagreb, Croatia
[92] Astrophysics Research Centre, School of Mathematics and Physics, Queen's University Belfast, Belfast BT7 1NN, UK
[93] Data Science and Big Data Lab, Pablo de Olavide University, 41013 Seville, Spain
[94] Institute of Astrophysics, FORTH, Crete, Greece
[95] Barcelona Supercomputing Center (BSC), Plaça Eusebi Güell 1–3, 08034 Barcelona, Spain
[96] ETSE Telecomunicación, Universidade de Vigo, Campus Lagoas-Marcosende, 36310 Vigo, Galicia, Spain
[97] F.R.S.-FNRS, Rue d'Egmont 5, 1000 Brussels, Belgium
[98] Asteroid Engineering Laboratory, Luleå University of Technology, Box 848, 981 28 Kiruna, Sweden
[99] Kapteyn Astronomical Institute, University of Groningen, Landleven 12, 9747 AD Groningen, The Netherlands
[100] IAC – Instituto de Astrofisica de Canarias, Via Láctea s/n, 38200 La Laguna S.C., Tenerife, Spain
[101] Department of Astrophysics, University of La Laguna, Via Láctea s/n, 38200 La Laguna S.C., Tenerife, Spain
[102] Astronomical Observatory, University of Warsaw, Al. Ujazdowskie 4, 00-478 Warszawa, Poland
[103] Research School of Astronomy & Astrophysics, Australian National University, Cotter Road, Weston, ACT 2611, Australia
[104] European Space Agency (ESA retired), European Space Research and Technology Centre (ESTEC), Keplerlaan 1, 2201AZ, Noordwijk, The Netherlands

[105] LESIA, Observatoire de Paris, Université PSL, CNRS, Sorbonne Université, Université de Paris, 5 place Jules Janssen, 92190 Meudon, France
[106] Université Rennes, CNRS, IPR (Institut de Physique de Rennes) – UMR 6251, 35000 Rennes, France
[107] INAF – Osservatorio Astronomico di Capodimonte, Via Moiariello 16, 80131, Napoli, Italy
[108] Shanghai Astronomical Observatory, Chinese Academy of Sciences, 80 Nandan Road, Shanghai 200030, PR China
[109] University of Chinese Academy of Sciences, No.19(A) Yuquan Road, Shijingshan District, Beijing 100049, PR China
[110] São Paulo State University, Grupo de Dinâmica Orbital e Planetologia, CEP 12516-410, Guaratinguetá, SP, Brazil
[111] Niels Bohr Institute, University of Copenhagen, Juliane Maries Vej 30, 2100 Copenhagen Ø, Denmark
[112] DXC Technology, Retortvej 8, 2500 Valby, Denmark
[113] Las Cumbres Observatory, 6740 Cortona Drive Suite 102, Goleta, CA 93117, USA
[114] CIGUS CITIC, Department of Nautical Sciences and Marine Engineering, University of A Coruña, Paseo de Ronda 51, 15071, A Coruña, Spain
[115] Astrophysics Research Institute, Liverpool John Moores University, 146 Brownlow Hill, Liverpool L3 5RF, UK
[116] IRAP, Université de Toulouse, CNRS, UPS, CNES, 9 Av. colonel Roche, BP 44346, 31028 Toulouse Cedex 4, France
[117] MTA CSFK Lendület Near-Field Cosmology Research Group, Konkoly Observatory, MTA Research Centre for Astronomy and Earth Sciences, Konkoly Thege Miklós út 15-17, 1121 Budapest, Hungary
[118] Pervasive Technologies s.l., c. Saragossa 118, 08006 Barcelona, Spain
[119] School of Physics and Astronomy, University of Leicester, University Road, Leicester LE1 7RH, UK
[120] Villanova University, Department of Astrophysics and Planetary Science, 800 E Lancaster Avenue, Villanova, PA 19085, USA
[121] Departmento de Física de la Tierra y Astrofísica, Universidad Complutense de Madrid, 28040 Madrid, Spain
[122] INAF – Osservatorio Astronomico di Brera, via E. Bianchi, 46, 23807 Merate (LC), Italy
[123] National Astronomical Observatory of Japan, 2-21-1 Osawa, Mitaka, Tokyo 181-8588, Japan
[124] Department of Particle Physics and Astrophysics, Weizmann Institute of Science, Rehovot 7610001, Israel
[125] Centre de Données Astronomique de Strasbourg, Strasbourg, France
[126] University of Exeter, School of Physics and Astronomy, Stocker Road, Exeter EX2 7SJ, UK
[127] Departamento de Astrofísica, Centro de Astrobiología (CSIC-INTA), ESA-ESAC. Camino Bajo del Castillo s/n, 28692 Villanueva de la Cañada, Madrid, Spain
[128] naXys, Department of Mathematics, University of Namur, Rue de Bruxelles 61, 5000 Namur, Belgium
[129] INAF–Osservatorio Astronomico di Trieste, via G.B. Tiepolo 11, 34131 Trieste, Italy
[130] Harvard-Smithsonian Center for Astrophysics, 60 Garden St., MS 15, Cambridge, MA 02138, USA
[131] H H Wills Physics Laboratory, University of Bristol, Tyndall Avenue, Bristol BS8 1TL, UK
[132] Escuela de Arquitectura y Politécnica – Universidad Europea de Valencia, Spain
[133] Escuela Superior de Ingeniería y Tecnología – Universidad Internacional de la Rioja, Spain
[134] Applied Physics Department, Universidade de Vigo, 36310 Vigo, Spain
[135] Instituto de Física e Ciencias Aeroespaciais (IFCAE), Universidade de Vigo, Á Campus de As Lagoas, 32004 Ourense, Spain
[136] Purple Mountain Observatory, Chinese Academy of Sciences, Nanjing 210023, PR China
[137] Sorbonne Université, CNRS, UMR7095, Institut d'Astrophysique de Paris, 98bis bd. Arago, 75014 Paris, France
[138] Faculty of Mathematics and Physics, University of Ljubljana, Jadranska ulica 19, 1000 Ljubljana, Slovenia
[139] Institute of Mathematics, École Polytechnique Fédérale de Lausanne (EPFL), Switzerland

Appendix A: Additional details on the classification of the catalog content

This FPR contains stellar sources displaying photometric and RV variability of different origins. In Sect. 3 we separated ellipsoidal variables from LPVs by comparing the amplitudes of their RV and G-band time series models. Then, among the LPV candidates, we found periods that result from pulsation as well as LSPs, and we tentatively distinguished the two types of variability in the G-band period-amplitude diagram. The separation of these two variability types in this diagram is not as clean as that between LPVs and ELLs in the G versus RV amplitude diagram. Therefore we examined in some more detail the two groups, in order to corroborate our classification.

We recall that, in absence of accurate and homogeneous knowledge about absolute brightness (i.e., distance), we have to rely on the variability parameters period and amplitude for this purpose. In addition to the variability parameters emerging from the analysis of the photometric time series, we can inspect the ones resulting from the RV curves. A combination of these four quantities is shown in Fig. A.1 (top panel), which displays the ratio between the semi-amplitude and the period of the G-band time series model against the same ratio for the RV time series model. For simplicity, we explicitly show the decimal logarithm of both quantities. There exists a clear correlation between the two ratios, indicating that the occurrence of a long period characterized by a small photometric amplitude is often associated with a relatively small RV amplitude as well.

The density contour lines in the top panel of Fig. A.1, as well as the histograms along the axes of the diagram, show that there are two regions of overdensity in the diagram. In order to better visualize them, in the bottom panel of Fig. A.1 we replaced the quantity on the vertical axis with its distance from the arbitrary reference line shown in the top panel. Fig. A.1 shows in two different colors the sources classified on the basis of Eq. (10). The latter is consistent with the distributions highlighted here with the inclusion of information related to RV variability, although it appears to lead to some contamination. It is possible that a classification that makes use of the periods and amplitudes resulting from both photometric and RV time series could help reduce such contamination. However, it would be more complex and less intuitive from a physical point of view, which supports the choice made in Sect. 3.

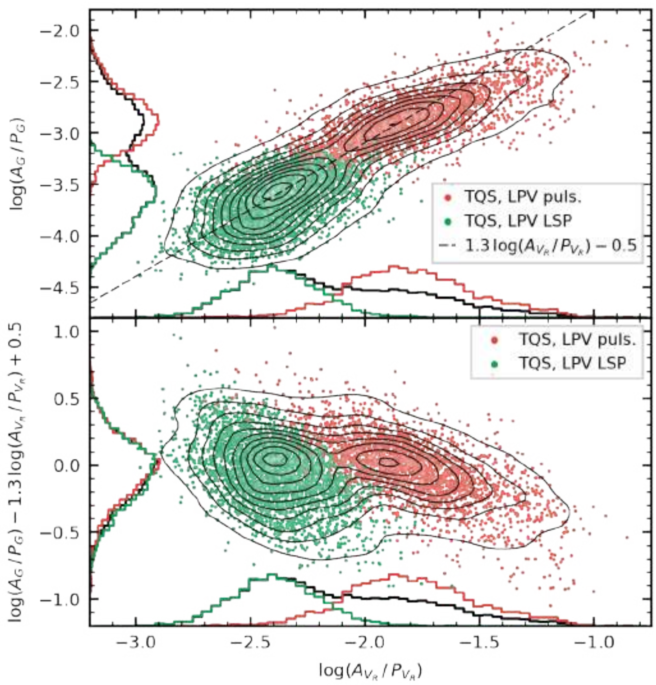

Fig. A.1. G-band versus RV period-amplitude ratios for the TQS sources classified as LPVs. Black contour lines represent a smoothed density map of the sample, and correspond to the black histograms on the sides of each panel. Each source is color-coded according to whether its period is identified as resulting from pulsation (red) or as an LSP (green). The same color-code is used for the histograms on the sides (normalized to their maximum). In the bottom panel the quantity $\log(A_G/P_G)$ is replaced with its distance from the dashed line displayed in the top panel, taken as an arbitrary reference.

Appendix B: Median RV in unevenly sampled time series

In this section we present a few representative examples of sources showing relatively large differences between the median RV and the zero-point RV, so that the former is not necessarily an accurate indicator of the center-of-mass velocity. The RV curves displayed in Fig. B.1 belong to sources with relatively long periods, for which *Gaia* observations cover only a few cycles. They also have large RV amplitudes and highly sinusoidal variations, indicating that their variability is due to binarity, and leaving little doubt concerning the authenticity of its physical origin. In all the examples displayed, the distribution of RV epochs is asymmetric as the phase near minimum RV is oversampled compared with other phases of the variability cycle. As a result, the median RV is underestimated, and shows a large difference with respect to V_R^0.

Further examples are provided in Fig. B.2, illustrating how the median of the RV time series ceases to be representative of the systemic RV due to the occurrence of clusters of RV epochs spanning an interval of time much shorter than the variability period of a given source. The RV distributions of the example time series are dominated by the effect of these groups causing large discrepancies between $\langle V_R \rangle$ and V_R^0, except in the fortuitous circumstances in which the clusters end up near the mid-point of the RV curve or cancel out with each other, as illustrated in panels (d) and (e) of Fig. B.2, respectively.

Overall, there exist rather specific circumstances in which the median $\langle V_R \rangle$ cannot be considered a good indicator of the systemic RV. These arise primarily from the uneven and irregular time sampling of *Gaia* observations, as well as the relatively small number of epochs, and affect mainly the sources with large RV amplitudes and long periods. In particular, when only a few variability cycles are covered, even a relatively homogeneous phase coverage can be insufficient to obtain a well-centered median value.

Appendix C: Numerical differences with respect to *Gaia* DR3

The production of this FPR required running the LPV variability pipeline on a subset of the sample of LPV candidates published as part of *Gaia* DR3. Despite having run the same operations on the photometric time series, we detected numerical differences with respect to the results previously obtained and published in *Gaia* DR3. We traced the origin of these numerical differences to the execution of the Apache Math Commons `LevenbergMarquardtOptimizer`, which produces different results depending on the adopted Java Development Kit

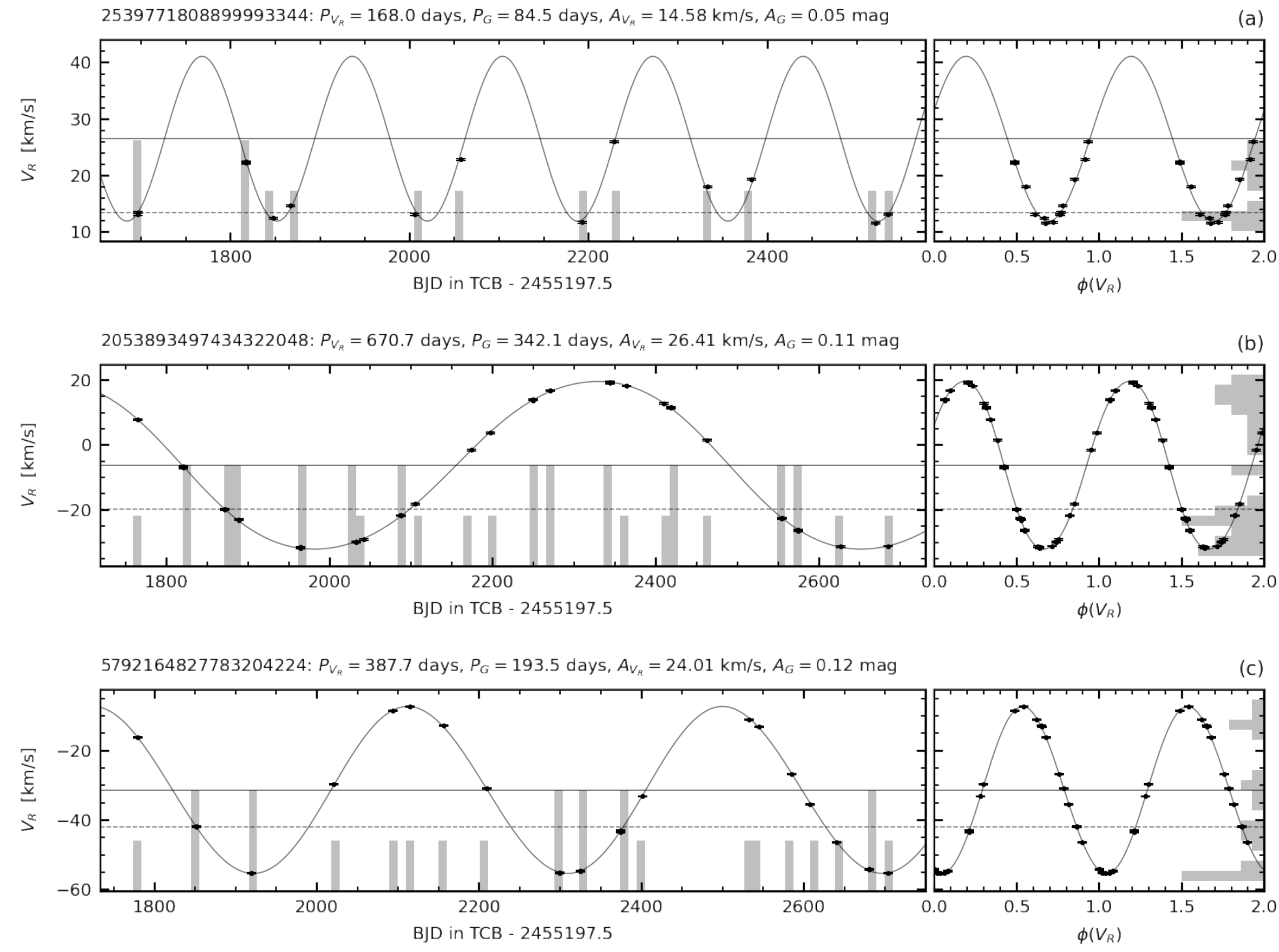

Fig. B.1. Examples of RV time series in which only a small number of cycles is covered, and the minimum phase is oversampled compared to other phases, leading the median RV to underestimate the systemic RV. In each row, the left panel shows the RV time series and best-fit model, whereas their folded counterparts are displayed in the right panel. Histograms in both panels aid to visualize the distribution of measurements both in time (to identify clustered measurements) and in RV. The solid and dashed lines mark the values of the zero-point and median RVs, respectively.

(JDK) version. The differences arised after updating from JDK-8 to JDK-17.

The differences are systematically reproducible[3], and a bug report was submitted to the Oracle bug submission system late in 2022, without receiving any feedback. The most plausible explanation we found for the numerical differences is that JDK-17 enforces the floating point standard IEEE 754, whereas in JDK-8 the runtime could decide to deviate from this standard in order to optimize the generated code[4].

In order to assess the impact of this bug we consider the periods of the *G*-band time series resulting from the variability pipeline before and after upgrading to JDK-17, and examine the differences between them. We use for this purpose the sample adopted for constructing the FPR catalog after pre-filtering that consists of 110 654 sources. From this set we exclude 1 413 sources for which either of the two periods is longer than the duration of the *G*-band time series. Within this reference set, 50% of the time series result in the exact same period regardless of the JDK version employed in the pipeline.

In Fig. C.1 we display the distribution of the relative difference between the JDK-8 and JDK-17 periods for the sources that have a non-null difference. It shows three well-distinct groups. About 60% of the time series display relative period differences that are at the level of machine precision, and thus entirely negligible ($< 10^{-13}$, and possibly zero). A second group contains sources that display relative differences between 10^{-13} and 10^{-5}, and consists of about 40% of the sample. In this case the absolute differences are on the order of a few minutes for periods of 1000 days, or a few seconds for periods of 10 days, hence they are negligible as well. Finally, there exists a third group containing fewer than 1% of the examined dataset, whose sources display relative period differences above 10^{-5}, but only 28 of them show a discrepancy above the 10% level (at most as large as 35%).

We examined the distribution of *G*-band time series statistics separately for these three groups, looking for systematic effects and features that might be triggering a strong effect of the bug. However, given the nature of this bug, one could expect it to impact different sources in a random fashion, and to be independent of the specific properties of the time series being processed.

[3] See the github repository https://github.com/gjevardat/ReproduceFloatingPointBug for an executable proof of the numerical differences.
[4] See https://openjdk.org/jeps/306 for more details.

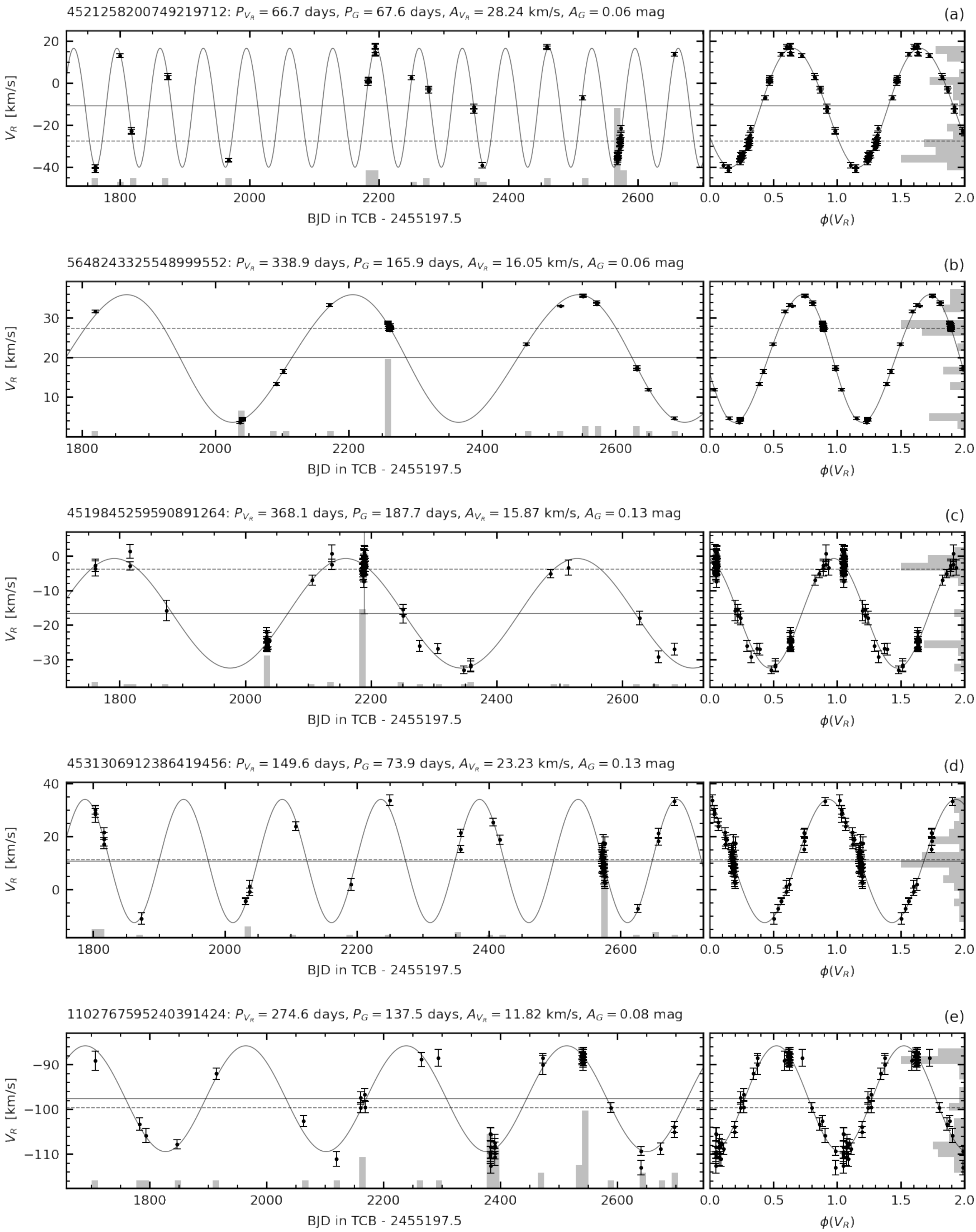

Fig. B.2. Similar to Fig. B.1, but showing examples of time series dominated by a large group of RV epochs spanning an interval of time much shorter than the typical period of the source, thereby distorting the time series statistics and causing a large difference between $\langle V_R \rangle$ and V_R^0. Cases (d) and (e) show examples where the clustered data points are, by chance, either located near the mid-point of the RV time series (case d), or cancel out with each other (case e).

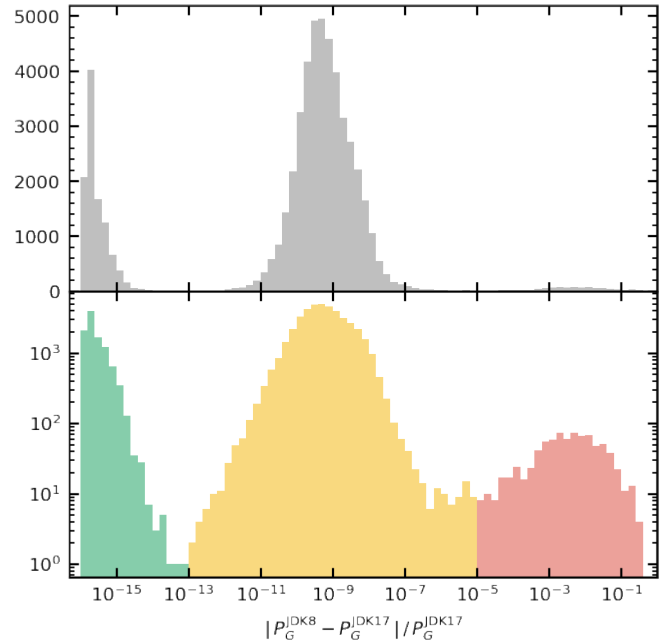

Fig. C.1. Distribution of relative differences between the period derived for G-band time series before and after the upgrade of the variability pipeline from JDK-8 to JDK-17. A linear scale is used in the top panel for the vertical axis, while a log-scale is used in the bottom panel. Three distinct groups are identified, colored in the bottom panel in green, orange and red, corresponding to various levels of difference. We note that only in the latter group the differences are non-negligible (being typically of order 1%). This group is so small that it is barely visible in the top panel.

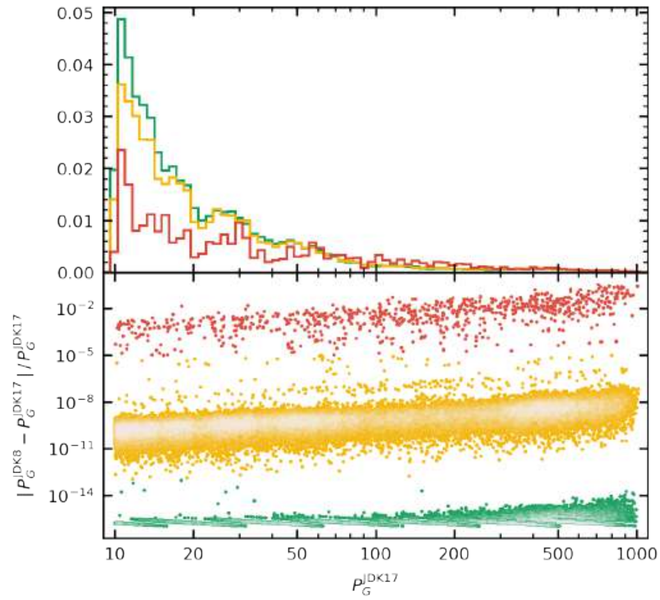

Fig. C.2. Period distribution for the three groups shown in Fig. C.1 (top panel), and relation of the period with the relative period difference. The period shown is the one obtained after the upgrade to JDK-17. The same color scheme as in Fig. C.1 is adopted. The histograms are normalized by area.

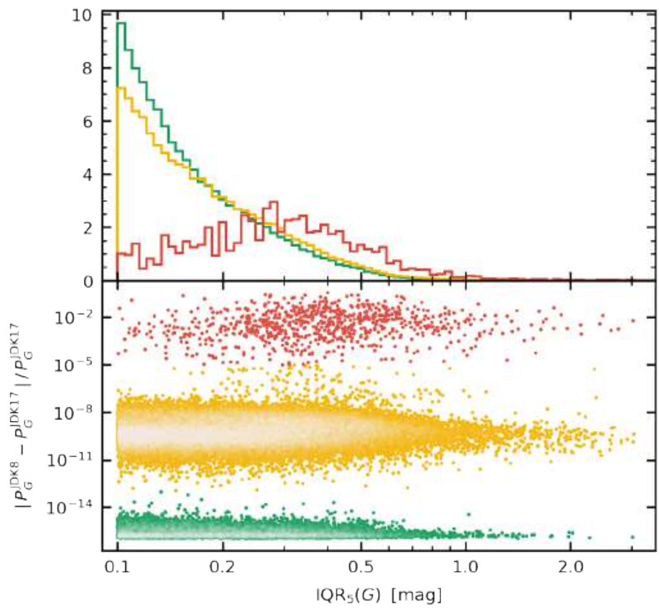

Fig. C.3. Similar to Fig. C.2, but for the 5–95% interquantile range of the G-band time series.

Our analysis tends to confirm this expectation. Overall, all three groups of sources show similar distributions of number of observations, time series duration, and average brightness. Only the parameters related with the amplitude and the period itself display a connection with the strength of the effect of the bug. In particular, there is a slight tendency for the third group (shown in red in Figs. C.2 and C.3) to lack sources with relatively small amplitudes and short periods, whereas the opposite is true for the first (green) group. Moreover, there is a clear correlation between the relative difference and the period within each group. The most likely explanation is that these sources are more exposed to numerical instabilities in the period determination as their time series cover a small number of cycles, which makes the period difficult to constrain in any case.

Appendix D: Catalog retrieval

Here are two examples on how to retrieve LPV-related data from the *Gaia* archive. A query like the following allows for retrieving selected quantities from the source catalog and LPV FPR catalog for all LPV FPR sources.

```
SELECT gs.source_id,
    gs.ra, gs.dec,
    fprlpv.frequency_rv, fprlpv.frequency_rv_error,
    fprlpv.amplitude_rv, fprlpv.flag_rv,
    ...
FROM gaiadr3.gaia_source AS gs
LEFT JOIN gaiafpr.vari_long_period_variable AS fprlpv
  ON gs.source_id = fprlpv.source_id
WHERE fprlpv.source_id IS NOT NULL
```

In order to retrieve all data from the source table, the LPV FPR table, the RV statistics table, and the tables of data on LPVs from DR3 for all sources published in the LPV FPR, a query like the following can be used.

```
SELECT src.*,
    fprlpv.*,
    rvstat.*,
    lpv.*,
    varistat.*
FROM gaiadr3.gaia_source AS src
LEFT JOIN gaiafpr.vari_long_period_variable AS fprlpv
```

```
    ON src.source_id = fprlpv.source_id
LEFT JOIN gaiafpr.vari_rad_vel_statistics AS rvstat
    ON src.source_id = rvstat.source_id
LEFT JOIN gaiadr3.vari_long_period_variable AS lpv
    ON src.source_id = lpv.source_id
LEFT JOIN gaiadr3.vari_summary AS varistat
    ON src.source_id = varistat.source_id
WHERE fprlpv.source_id IS NOT NULL
```

Finally, one can download all the RV time series published as part of this FPR using a source like the following.

```
SELECT fprlpv.source_id,
    varirv.transit_id,
    varirv.rv_obs_time,
    varirv.radial_velocity,
    varirv.radial_velocity_error
    varirv.rejected_by_variability
FROM gaiafpr.vari_long_period_variable AS fprlpv
LEFT JOIN gaiafpr.vari_epoch_radial_velocity AS varirv
    ON fprlpv.source_id = varirv.source_id
WHERE fprlpv.source_id IS NOT NULL
```

We also recall that it is possible to download ancillary data such as the RV and photometric time series using the *Gaia* datalink service[5].

Appendix E: Acknowledgements

This work presents results from the European Space Agency (ESA) space mission *Gaia*. *Gaia* data are being processed by the *Gaia* Data Processing and Analysis Consortium (DPAC). Funding for the DPAC is provided by national institutions, in particular the institutions participating in the *Gaia* MultiLateral Agreement (MLA). The *Gaia* mission website is https://www.cosmos.esa.int/gaia. The *Gaia* archive website is https://archives.esac.esa.int/gaia.

The *Gaia* mission and data processing have financially been supported by, in alphabetical order by country:

- the Algerian Centre de Recherche en Astronomie, Astrophysique et Géophysique of Bouzareah Observatory;
- the Austrian Fonds zur Förderung der wissenschaftlichen Forschung (FWF) Hertha Firnberg Programme through grants T359, P20046, and P23737;
- the BELgian federal Science Policy Office (BELSPO) through various PROgramme de Développement d'Expériences scientifiques (PRODEX) grants of the European Space Agency (ESA), the Research Foundation Flanders (Fonds Wetenschappelijk Onderzoek) through grant VS.091.16N, the Fonds de la Recherche Scientifique (FNRS), and the Research Council of Katholieke Universiteit (KU) Leuven through grant C16/18/005 (Pushing AsteRoseismology to the next level with TESS, GaiA, and the Sloan DIgital Sky SurvEy – PARADISE);
- the Brazil-France exchange programmes Fundação de Amparo à Pesquisa do Estado de São Paulo (FAPESP) and Coordenação de Aperfeicoamento de Pessoal de Nível Superior (CAPES) - Comité Français d'Evaluation de la Coopération Universitaire et Scientifique avec le Brésil (COFECUB);
- the Chilean Agencia Nacional de Investigación y Desarrollo (ANID) through Fondo Nacional de Desarrollo Científico y Tecnológico (FONDECYT) Regular Project 1210992 (L. Chemin);
- the National Natural Science Foundation of China (NSFC) through grants 11573054, 11703065, and 12173069, the China Scholarship Council through grant 201806040200, and the Natural Science Foundation of Shanghai through grant 21ZR1474100;
- the Tenure Track Pilot Programme of the Croatian Science Foundation and the École Polytechnique Fédérale de Lausanne and the project TTP-2018-07-1171 'Mining the Variable Sky', with the funds of the Croatian-Swiss Research Programme;
- the Czech-Republic Ministry of Education, Youth, and Sports through grant LG 15010 and INTER-EXCELLENCE grant LTAUSA18093, and the Czech Space Office through ESA PECS contract 98058;
- the Danish Ministry of Science;
- the Estonian Ministry of Education and Research through grant IUT40-1;
- the European Commission's Sixth Framework Programme through the European Leadership in Space Astrometry (ELSA) Marie Curie Research Training Network (MRTN-CT-2006-033481), through Marie Curie project PIOF-GA-2009-255267 (Space AsteroSeismology & RR Lyrae stars, SAS-RRL), and through a Marie Curie Transfer-of-Knowledge (ToK) fellowship (MTKD-CT-2004-014188); the European Commission's Seventh Framework Programme through grant FP7-606740 (FP7-SPACE-2013-1) for the *Gaia* European Network for Improved data User Services (GENIUS) and through grant 264895 for the *Gaia* Research for European Astronomy Training (GREAT-ITN) network;
- the European Cooperation in Science and Technology (COST) through COST Action CA18104 'Revealing the Milky Way with *Gaia* (MW-*Gaia*)';
- the European Research Council (ERC) through grants 320360, 647208, and 834148 and through the European Union's Horizon 2020 research and innovation and excellent science programmes through Marie Skłodowska-Curie grants 687378 (Small Bodies: Near and Far), 682115 (Using the Magellanic Clouds to Understand the Interaction of Galaxies), 695099 (A sub-percent distance scale from binaries and Cepheids – CepBin), 716155 (Structured ACCREtion Disks – SACCRED), 745617 (Our Galaxy at full HD – Gal-HD), 895174 (The build-up and fate of self-gravitating systems in the Universe), 951549 (Sub-percent calibration of the extragalactic distance scale in the era of big surveys – UniverScale), 101004214 (Innovative Scientific Data Exploration and Exploitation Applications for Space Sciences – EXPLORE), 101004719 (OPTICON-RadioNET Pilot), 101055318 (The 3D motion of the Interstellar Medium with ESO and ESA telescopes – ISM-FLOW), and 101063193 (Evolutionary Mechanisms in the Milky waY; the Gaia Data Release 3 revolution – EMMY);
- the European Science Foundation (ESF), in the framework of the *Gaia* Research for European Astronomy Training Research Network Programme (GREAT-ESF);
- the European Space Agency (ESA) in the framework of the *Gaia* project, through the Plan for European Cooperating States (PECS) programme through contracts C98090 and 4000106398/12/NL/KML for Hungary, through contract 4000115263/15/NL/IB for Germany, through PROgramme de Développement d'Expériences scientifiques (PRODEX) grants 4000132054 for Hungary and through contract 4000132226/20/ES/CM;
- the Academy of Finland through grants 299543, 307157, 325805, 328654, 336546, and 345115 and the Magnus Ehrnrooth Foundation;

[5] https://www.cosmos.esa.int/web/gaia-users/archive/datalink-products

- the French Centre National d'Études Spatiales (CNES), the Agence Nationale de la Recherche (ANR) through grant ANR-10-IDEX-0001-02 for the 'Investissements d'avenir' programme, through grant ANR-15-CE31-0007 for project 'Modelling the Milky Way in the *Gaia* era' (MOD4*Gaia*), through grant ANR-14-CE33-0014-01 for project 'The Milky Way disc formation in the *Gaia* era' (ARCHEOGAL), through grant ANR-15-CE31-0012-01 for project 'Unlocking the potential of Cepheids as primary distance calibrators' (UnlockCepheids), through grant ANR-19-CE31-0017 for project 'Secular evolution of galaxies' (SEGAL), and through grant ANR-18-CE31-0006 for project 'Galactic Dark Matter' (GaDaMa), the Centre National de la Recherche Scientifique (CNRS) and its SNO *Gaia* of the Institut des Sciences de l'Univers (INSU), its Programmes Nationaux: Cosmologie et Galaxies (PNCG), Gravitation Références Astronomie Métrologie (PNGRAM), Planétologie (PNP), Physique et Chimie du Milieu Interstellaire (PCMI), and Physique Stellaire (PNPS), supported by INSU along with the Institut National de Physique (INP) and the Institut National de Physique nucléaire et de Physique des Particules (IN2P3), and co-funded by CNES; the 'Action Fédératrice *Gaia*' of the Observatoire de Paris, and the Région de Franche-Comté;
- the German Aerospace Agency (Deutsches Zentrum für Luft- und Raumfahrt e.V., DLR) through grants 50QG0501, 50QG0601, 50QG0602, 50QG0701, 50QG0901, 50QG1001, 50QG1101, 50QG1401, 50QG1402, 50QG1403, 50QG1404, 50QG1904, 50QG2101, 50QG2102, and 50QG2202, and the Centre for Information Services and High Performance Computing (ZIH) at the Technische Universität Dresden for generous allocations of computer time;
- the Hungarian Academy of Sciences through the János Bolyai Research Scholarship (G. Marton and Z. Nagy), the Lendület Programme grants LP2014-17 and LP2018-7 and the Hungarian National Research, Development, and Innovation Office (NKFIH) through grant KKP-137523 ('SeismoLab');
- the Science Foundation Ireland (SFI) through a Royal Society - SFI University Research Fellowship (M. Fraser);
- the Israel Ministry of Science and Technology through grant 3-18143 and the Israel Science Foundation (ISF) through grant 1404/22;
- the Agenzia Spaziale Italiana (ASI) through contracts I/037/08/0, I/058/10/0, 2014-025-R.0, 2014-025-R.1.2015, and 2018-24-HH.0 and its addendum 2018-24-HH.1-2022 to the Italian Istituto Nazionale di Astrofisica (INAF), contract 2014-049-R.0/1/2, 2022-14-HH.0 to INAF for the Space Science Data Centre (SSDC, formerly known as the ASI Science Data Center, ASDC), contracts I/008/10/0, 2013/030/I.0, 2013-030-I.0.1-2015, and 2016-17-I.0 to the Aerospace Logistics Technology Engineering Company (ALTEC S.p.A.), INAF, and the Italian Ministry of Education, University, and Research (Ministero dell'Istruzione, dell'Università e della Ricerca) through the Premiale project 'MIning The Cosmos Big Data and Innovative Italian Technology for Frontier Astrophysics and Cosmology' (MITiC);
- the Netherlands Organisation for Scientific Research (NWO) through grant NWO-M-614.061.414, through a VICI grant (A. Helmi), and through a Spinoza prize (A. Helmi), and the Netherlands Research School for Astronomy (NOVA);
- the Polish National Science Centre through HARMONIA grant 2018/30/M/ST9/00311 and DAINA grant 2017/27/L/ST9/03221 and the Ministry of Science and Higher Education (MNiSW) through grant DIR/WK/2018/12;
- the Portuguese Fundação para a Ciência e a Tecnologia (FCT) through national funds, grants 2022.06962.PTDC and 2022.03993.PTDC, and work contract DL 57/2016/CP1364/CT0006, grants UIDB/04434/2020 and UIDP/04434/2020 for the Instituto de Astrofísica e Ciências do Espaço (IA), grants UIDB/00408/2020 and UIDP/00408/2020 for LASIGE, and grants UIDB/00099/2020 and UIDP/00099/2020 for the Centro de Astrofísica e Gravitação (CENTRA);
- the Slovenian Research Agency through grant P1-0188;
- the Spanish Ministry of Economy (MINECO/FEDER, UE), the Spanish Ministry of Science and Innovation (MCIN), the Spanish Ministry of Education, Culture, and Sports, and the Spanish Government through grants BES-2016-078499, BES-2017-083126, BES-C-2017-0085, ESP2016-80079-C2-1-R, FPU16/03827, RTI2018-095076-B-C22, PID2021-122842OB-C22, PDC2021-121059-C22, and TIN2015-65316-P ('Computación de Altas Prestaciones VII'), the Juan de la Cierva Incorporación Programme (FJCI-2015-2671 and IJC2019-04862-I for F. Anders), the Severo Ochoa Centre of Excellence Programme (SEV2015-0493) and MCIN/AEI/10.13039/501100011033/EU FEDER and Next Generation EU/PRTR (PRTR-C17.I1); the European Union through European Regional Development Fund 'A way of making Europe' through grants PID2021-122842OB-C21, PID2021-125451NA-I00, CNS2022-13523 and RTI2018-095076-B-C21, the Institute of Cosmos Sciences University of Barcelona (ICCUB, Unidad de Excelencia 'María de Maeztu') through grant CEX2019-000918-M, the University of Barcelona's official doctoral programme for the development of an R+D+i project through an Ajuts de Personal Investigador en Formació (APIF) grant, the Spanish Virtual Observatory project funded by MCIN/AEI/10.13039/501100011033/ through grant PID2020-112949GB-I00; the Centro de Investigación en Tecnologías de la Información y las Comunicaciones (CITIC), funded by the Xunta de Galicia through the collaboration agreement to reinforce CIGUS research centers, research consolidation grant ED431B 2021/36 and scholarships from Xunta de Galicia and the EU - ESF ED481A-2019/155 and ED481A 2021/296; the Red Española de Supercomputación (RES) computer resources at MareNostrum, the Barcelona Supercomputing Centre - Centro Nacional de Supercomputación (BSC-CNS) through activities AECT-2017-2-0002, AECT-2017-3-0006, AECT-2018-1-0017, AECT-2018-2-0013, AECT-2018-3-0011, AECT-2019-1-0010, AECT-2019-2-0014, AECT-2019-3-0003, AECT-2020-1-0004, and DATA-2020-1-0010, the Departament d'Innovació, Universitats i Empresa de la Generalitat de Catalunya through grant 2014-SGR-1051 for project 'Models de Programació i Entorns d'Execució Parallels' (MPEXPAR), and Ramon y Cajal Fellowships RYC2018-025968-I, RYC2021-031683-I and RYC2021-033762-I, funded by MICIN/AEI/10.13039/501100011033 and by the European Union NextGenerationEU/PRTR and the European Science Foundation ('Investing in your future'); the Port d'Informació Científica (PIC), through a collaboration between the Centro de Investigaciones Energéticas, Medioambientales y Tecnológicas (CIEMAT) and the Institut de Física d'Altes Energies (IFAE), supported by the call for grants for Scientific and Technical Equipment 2021 of the State Program for Knowledge Generation and Scientific and Technological Strengthening of the R+D+i

System, financed by MCIN/AEI/ 10.13039/501100011033 and the EU NextGeneration/PRTR (Hadoop Cluster for the comprehensive management of massive scientific data, reference EQC2021-007479-P);
- the Swedish National Space Agency (SNSA/Rymdstyrelsen);
- the Swiss State Secretariat for Education, Research, and Innovation through the Swiss Activités Nationales Complémentaires and the Swiss National Science Foundation through an Eccellenza Professorial Fellowship (award PCEFP2_194638 for R. Anderson);
- the United Kingdom Particle Physics and Astronomy Research Council (PPARC), the United Kingdom Science and Technology Facilities Council (STFC), and the United Kingdom Space Agency (UKSA) through the following grants to the University of Bristol, Brunel University London, the Open University, the University of Cambridge, the University of Edinburgh, the University of Leicester, the Mullard Space Sciences Laboratory of University College London, and the United Kingdom Rutherford Appleton Laboratory (RAL): PP/D006503/1, PP/D006511/1, PP/D006546/1, PP/D006570/1, PP/D006791/1, ST/I000852/1, ST/J005045/1, ST/K00056X/1, ST/K000209/1, ST/K000756/1, ST/K000578/1, ST/L002388/1, ST/L006553/1, ST/L006561/1, ST/N000595/1, ST/N000641/1, ST/N000978/1, ST/N001117/1, ST/S000089/1, ST/S000976/1, ST/S000984/1, ST/S001123/1, ST/S001948/1, ST/S001980/1, ST/S002103/1, ST/V000969/1, ST/W002469/1, ST/W002493/1, ST/W002671/1, ST/W002809/1, EP/V520342/1, ST/X00158X/1, ST/X001601/1, ST/X001636/1, ST/X001687/1, ST/X002667/1, ST/X002683/1 and ST/X002969/1.

The *Gaia* project and data processing have made use of:
- the Set of Identifications, Measurements, and Bibliography for Astronomical Data (SIMBAD, Wenger et al. 2000), the 'Aladin sky atlas' (Bonnarel et al. 2000; Boch & Fernique 2014), and the VizieR catalogue access tool (Ochsenbein et al. 2000), all operated at the Centre de Données astronomiques de Strasbourg (CDS);
- the National Aeronautics and Space Administration (NASA) Astrophysics Data System (ADS);
- the SPace ENVironment Information System (SPENVIS), initiated by the Space Environment and Effects Section (TEC-EES) of ESA and developed by the Belgian Institute for Space Aeronomy (BIRA-IASB) under ESA contract through ESA's General Support Technologies Programme (GSTP), administered by the BELgian federal Science Policy Office (BELSPO);
- the software products TOPCAT, STIL, and STILTS (Taylor 2005, 2006);
- Matplotlib (Hunter 2007);
- IPython (Pérez & Granger 2007);
- Astropy, a community-developed core Python package for Astronomy (Astropy Collaboration et al. 2018);
- R (R Core Team 2013);
- the HEALPix package (Górski et al. 2005, http://healpix.sourceforge.net/);
- Vaex (Breddels & Veljanoski 2018);
- the Hipparcos-2 catalogue (van Leeuwen 2007). The Hipparcos and Tycho catalogues were constructed under the responsibility of large scientific teams collaborating with ESA. The Consortia Leaders were Lennart Lindegren (Lund, Sweden: NDAC) and Jean Kovalevsky (Grasse, France: FAST), together responsible for the Hipparcos Catalogue; Erik Høg (Copenhagen, Denmark: TDAC) responsible for the Tycho Catalogue; and Catherine Turon (Meudon, France: INCA) responsible for the Hipparcos Input Catalogue (HIC);
- the Tycho-2 catalogue (Høg et al. 2000), the construction of which was supported by the Velux Foundation of 1981 and the Danish Space Board;
- The Tycho double star catalogue (TDSC, Fabricius et al. 2002), based on observations made with the ESA Hipparcos astrometry satellite, as supported by the Danish Space Board and the United States Naval Observatory through their double-star programme;
- data products from the Two Micron All Sky Survey (2MASS, Skrutskie et al. 2006), which is a joint project of the University of Massachusetts and the Infrared Processing and Analysis Center (IPAC) / California Institute of Technology, funded by the National Aeronautics and Space Administration (NASA) and the National Science Foundation (NSF) of the USA;
- the ninth data release of the AAVSO Photometric All-Sky Survey (APASS, Henden et al. 2016), funded by the Robert Martin Ayers Sciences Fund;
- the first data release of the Pan-STARRS survey (Chambers et al. 2016; Magnier et al. 2020a; Waters et al. 2020; Magnier et al. 2020c,b; Flewelling et al. 2020). The Pan-STARRS1 Surveys (PS1) and the PS1 public science archive have been made possible through contributions by the Institute for Astronomy, the University of Hawaii, the Pan-STARRS Project Office, the Max-Planck Society and its participating institutes, the Max Planck Institute for Astronomy, Heidelberg and the Max Planck Institute for Extraterrestrial Physics, Garching, The Johns Hopkins University, Durham University, the University of Edinburgh, the Queen's University Belfast, the Harvard-Smithsonian Center for Astrophysics, the Las Cumbres Observatory Global Telescope Network Incorporated, the National Central University of Taiwan, the Space Telescope Science Institute, the National Aeronautics and Space Administration (NASA) through grant NNX08AR22G issued through the Planetary Science Division of the NASA Science Mission Directorate, the National Science Foundation through grant AST-1238877, the University of Maryland, Eotvos Lorand University (ELTE), the Los Alamos National Laboratory, and the Gordon and Betty Moore Foundation;
- the second release of the Guide Star Catalogue (GSC2.3, Lasker et al. 2008). The Guide Star Catalogue II is a joint project of the Space Telescope Science Institute (STScI) and the Osservatorio Astrofisico di Torino (OATo). STScI is operated by the Association of Universities for Research in Astronomy (AURA), for the National Aeronautics and Space Administration (NASA) under contract NAS5-26555. OATo is operated by the Italian National Institute for Astrophysics (INAF). Additional support was provided by the European Southern Observatory (ESO), the Space Telescope European Coordinating Facility (STECF), the International GEMINI project, and the European Space Agency (ESA) Astrophysics Division (nowadays SCI-S);
- the eXtended, Large (XL) version of the catalogue of Positions and Proper Motions (PPM-XL, Roeser et al. 2010);
- data products from the Wide-field Infrared Survey Explorer (WISE), which is a joint project of the University of California, Los Angeles, and the Jet Propulsion Laboratory/California Institute of Technology, and

NEOWISE, which is a project of the Jet Propulsion Laboratory/California Institute of Technology. WISE and NEOWISE are funded by the National Aeronautics and Space Administration (NASA);
– the first data release of the United States Naval Observatory (USNO) Robotic Astrometric Telescope (URAT-1, Zacharias et al. 2015);
– the fourth data release of the United States Naval Observatory (USNO) CCD Astrograph Catalogue (UCAC-4, Zacharias et al. 2013);
– the sixth and final data release of the Radial Velocity Experiment (RAVE DR6, Steinmetz et al. 2020a,b). Funding for RAVE has been provided by the Leibniz Institute for Astrophysics Potsdam (AIP), the Australian Astronomical Observatory, the Australian National University, the Australian Research Council, the French National Research Agency, the German Research Foundation (SPP 1177 and SFB 881), the European Research Council (ERC-StG 240271 Galactica), the Istituto Nazionale di Astrofisica at Padova, the Johns Hopkins University, the National Science Foundation of the USA (AST-0908326), the W.M. Keck foundation, the Macquarie University, the Netherlands Research School for Astronomy, the Natural Sciences and Engineering Research Council of Canada, the Slovenian Research Agency, the Swiss National Science Foundation, the Science & Technology Facilities Council of the UK, Opticon, Strasbourg Observatory, and the Universities of Basel, Groningen, Heidelberg, and Sydney. The RAVE website is at https://www.rave-survey.org/;
– the first data release of the Large sky Area Multi-Object Fibre Spectroscopic Telescope (LAMOST DR1, Luo et al. 2015);
– the K2 Ecliptic Plane Input Catalogue (EPIC, Huber et al. 2016);
– the ninth data release of the Sloan Digitial Sky Survey (SDSS DR9, Ahn et al. 2012). Funding for SDSS-III has been provided by the Alfred P. Sloan Foundation, the Participating Institutions, the National Science Foundation, and the United States Department of Energy Office of Science. The SDSS-III website is http://www.sdss3.org/. SDSS-III is managed by the Astrophysical Research Consortium for the Participating Institutions of the SDSS-III Collaboration including the University of Arizona, the Brazilian Participation Group, Brookhaven National Laboratory, Carnegie Mellon University, University of Florida, the French Participation Group, the German Participation Group, Harvard University, the Instituto de Astrofísica de Canarias, the Michigan State/Notre Dame/JINA Participation Group, Johns Hopkins University, Lawrence Berkeley National Laboratory, Max Planck Institute for Astrophysics, Max Planck Institute for Extraterrestrial Physics, New Mexico State University, New York University, Ohio State University, Pennsylvania State University, University of Portsmouth, Princeton University, the Spanish Participation Group, University of Tokyo, University of Utah, Vanderbilt University, University of Virginia, University of Washington, and Yale University;
– the thirteenth release of the Sloan Digital Sky Survey (SDSS DR13, Albareti et al. 2017). Funding for SDSS-IV has been provided by the Alfred P. Sloan Foundation, the United States Department of Energy Office of Science, and the Participating Institutions. SDSS-IV acknowledges support and resources from the Center for High-Performance Computing at the University of Utah. The SDSS web site is https://www.sdss.org/. SDSS-IV is managed by the Astrophysical Research Consortium for the Participating Institutions of the SDSS Collaboration including the Brazilian Participation Group, the Carnegie Institution for Science, Carnegie Mellon University, the Chilean Participation Group, the French Participation Group, Harvard-Smithsonian Center for Astrophysics, Instituto de Astrofísica de Canarias, The Johns Hopkins University, Kavli Institute for the Physics and Mathematics of the Universe (IPMU) / University of Tokyo, the Korean Participation Group, Lawrence Berkeley National Laboratory, Leibniz Institut für Astrophysik Potsdam (AIP), Max-Planck-Institut für Astronomie (MPIA Heidelberg), Max-Planck-Institut für Astrophysik (MPA Garching), Max-Planck-Institut für Extraterrestrische Physik (MPE), National Astronomical Observatories of China, New Mexico State University, New York University, University of Notre Dame, Observatário Nacional / MCTI, The Ohio State University, Pennsylvania State University, Shanghai Astronomical Observatory, United Kingdom Participation Group, Universidad Nacional Autónoma de México, University of Arizona, University of Colorado Boulder, University of Oxford, University of Portsmouth, University of Utah, University of Virginia, University of Washington, University of Wisconsin, Vanderbilt University, and Yale University;
– the second release of the SkyMapper catalogue (SkyMapper DR2, Onken et al. 2019, Digital Object Identifier 10.25914/5ce60d31ce759). The national facility capability for SkyMapper has been funded through grant LE130100104 from the Australian Research Council (ARC) Linkage Infrastructure, Equipment, and Facilities (LIEF) programme, awarded to the University of Sydney, the Australian National University, Swinburne University of Technology, the University of Queensland, the University of Western Australia, the University of Melbourne, Curtin University of Technology, Monash University, and the Australian Astronomical Observatory. SkyMapper is owned and operated by The Australian National University's Research School of Astronomy and Astrophysics. The survey data were processed and provided by the SkyMapper Team at the Australian National University. The SkyMapper node of the All-Sky Virtual Observatory (ASVO) is hosted at the National Computational Infrastructure (NCI). Development and support the SkyMapper node of the ASVO has been funded in part by Astronomy Australia Limited (AAL) and the Australian Government through the Commonwealth's Education Investment Fund (EIF) and National Collaborative Research Infrastructure Strategy (NCRIS), particularly the National eResearch Collaboration Tools and Resources (NeCTAR) and the Australian National Data Service Projects (ANDS);
– the *Gaia*-ESO Public Spectroscopic Survey (GES, Gilmore et al. 2022; Randich et al. 2022). The *Gaia*-ESO Survey is based on data products from observations made with ESO Telescopes at the La Silla Paranal Observatory under programme ID 188.B-3002. Public data releases are available through the ESO Science Portal. The project has received funding from the Leverhulme Trust (project RPG-2012-541), the European Research Council (project ERC-2012-AdG 320360-*Gaia*-ESO-MW), and the Istituto Nazionale di Astrofisica, INAF (2012: CRA 1.05.01.09.16; 2013: CRA 1.05.06.02.07).

The GBOT programme (GBOT) uses observations collected at (i) the European Organisation for Astronomical Research in the Southern Hemisphere (ESO) with the VLT Survey Telescope (VST), under ESO programmes 092.B-0165, 093.B-0236, 094.B-0181, 095.B-0046, 096.B-0162, 097.B-0304, 098.B-0030, 099.B-0034, 0100.B-0131, 0101.B-0156, 0102.B-0174, 0103.B-0165, 0104.B-0081, 0106.20ZA.001 (OmegaCam), 0106.20ZA.002 (FORS2), 0108.21YF; and under INAF programs 110.256C, 112.266Q; and (ii) the Liverpool Telescope, which is operated on the island of La Palma by Liverpool John Moores University in the Spanish Observatorio del Roque de los Muchachos of the Instituto de Astrofísica de Canarias with financial support from the United Kingdom Science and Technology Facilities Council, and (iii) telescopes of the Las Cumbres Observatory Global Telescope Network.

In addition to the currently active DPAC (and ESA science) authors of the peer-reviewed papers accompanying the data release, there are large numbers of former DPAC members who made significant contributions to the (preparations of the) data processing. In addition to the DPAC consortium, past and present, there are numerous people, mostly in ESA and in industry, who have made or continue to make essential contributions to *Gaia*, for instance those employed in science and mission operations or in the design, manufacturing, integration, and testing of the spacecraft and its modules, subsystems, and units. Many of those will remain unnamed yet spent countless hours, occasionally during nights, weekends, and public holidays, in cold offices and dark clean rooms. They are acknowledged in the Gaia Documentation